PLOS Neglected Tropical Diseases

RESEARCH ARTICLE

Distinct temporal patterns of liver immune responses to pathogenic and non-pathogenic *Entamoeba histolytica* clones

Helena Fehling[1,2☯], Johannes Allweier[2☯], Barbara Honecker[1☯], Claudia Marggraff[1], Michel-Ruben Glagowski[2], Juliett Anders[2], Hannelore Lotter[1], Iris Bruchhaus[2,3*]

1 RG Molecular Infection Immunology, Bernhard Nocht Institute for Tropical Medicine, Hamburg, Germany,
2 RG Host-Parasite Interaction, Bernhard Nocht Institute for Tropical Medicine, Hamburg, Germany,
3 Department of Biology, University of Hamburg, Hamburg, Germany

☯ These authors contributed equally to this work
* bruchhaus@bnitm.de

Check for updates

OPEN ACCESS

Citation: Fehling H, Allweier J, Honecker B, Marggraff C, Glagowski M-R, Anders J, et al. (2026) Distinct temporal patterns of liver immune responses to pathogenic and non-pathogenic *Entamoeba histolytica* clones. PLoS Negl Trop Dis 20(11): e0014869. https://doi.org/10.1371/journal.pntd.0014869

Editor: Maria Fantinatti, Universidade do Estado do Rio de Janeiro, BRAZIL

Received: May 19, 2026

Accepted: October 29, 2026

Published: November 10, 2026

Peer Review History: PLOS recognizes the benefits of transparency in the peer review process; therefore, we enable the publication of all of the content of peer review and author responses alongside final, published articles. The editorial history of this article is available here: https://doi.org/10.1371/journal.pntd.0014869

Copyright: © 2026 Fehling et al. This is an open access article distributed under the terms of the Creative Commons Attribution License, which permits unrestricted use, distribution,

Abstract

Entamoeba histolytica is a protozoan parasite that can cause severe liver disease known as amoebic liver abscess. However, only a subset of infected individuals develops invasive disease, indicating that host-parasite interactions are critical determinants of disease outcome. In this study, we investigated the clone-specific modulation of hepatic immune responses using non-pathogenic A1^{np} and pathogenic B2^{p} *E. histolytica* clones. Time-resolved transcriptome analyses (6, 12, 24 hours post-infection) in a murine model revealed distinct immune trajectories. Both clones activated innate immune pathways early after infection, but their responses differed markedly in magnitude and composition. A1^{np} infection induced a rapid and controlled inflammatory response associated with antimicrobial activity and resolution-promoting signalling. In contrast, B2^{p} infection triggered a stronger and more complex immune response characterised by pronounced cytokine and chemokine expression, activation of stress and redox pathways, and tissue remodelling processes. The B2^{p} induced response exhibited features of excessive immune activation, accompanied by the upregulation of counter-regulation genes such as *Ackr2*. These findings indicate that liver pathology is not solely determined by parasite presence, but rather may also be influenced by the nature and regulation of the host immune response. Overall, the observed differences between A1^{np} and B2^{p} infections suggest that parasite-specific properties shape hepatic immune activation and may influence disease progression.

Author summary

Although infection with the parasite *Entamoeba histolytica* can lead to severe liver disease, most infected individuals remain asymptomatic. This suggests that

and reproduction in any medium, provided the original author and source are credited.

Data availability statement: The RNA sequencing datasets generated during the current study are available in the Gene Expression Omnibus (GEO) repository under accession number [GSE329300].

Funding: The work was supported by grants of the Deutsche Forschungsgemeinschaft (BR 1744/17-2 to IB and CRC 841 (Liver inflammation: Infection, immune regulation and Consequences) to HL) and Jürgen Manchot Stiftung (to MRG). MRG received a doctoral scholarship from the Jürgen Manchot Foundation to support his PhD research. The funders had no role in study design, data collection and analysis, decision to publish, or preparation of the manuscript.

Competing interests: The authors have declared that no competing interests exist.

the outcome of the disease is not determined solely by the parasite, but also by how the host responds to the infection. In this study, we used a mouse model to compare how the liver reacts to infection with two *E. histolytica* clones that differ in their ability to cause amoebic liver abscesses. Using this model and time-resolved transcriptome analysis, we found that both clones trigger an early immune response; however, the nature of this response differs markedly. The non-pathogenic clone induced a rapid and controlled reaction associated with antimicrobial defence and tissue protection. In contrast, the pathogenic clone provoked a stronger and more prolonged inflammatory response accompanied by cellular stress and tissue remodelling processes. Notably, this heightened response also activated regulatory mechanisms that attempted to limit excessive inflammation. Our findings demonstrate that differences in disease severity are linked to the activation and regulation of the host immune system, rather than simply to the presence of the parasite.

Introduction

Entamoeba histolytica is a protozoan parasite that causes intestinal and extraintestinal disease in humans. While most infections are asymptomatic, around 10% of affected individuals develop invasive manifestations, such as amoebic colitis or amoebic liver abscess (ALAs). The latter represents one of the most severe complications, accounting for substantial morbidity and mortality, particularly in endemic regions of Asia, Africa and Latin America, with an estimated 26,000 deaths worldwide in 2016 [1].

The life cycle of *E. histolytica* includes infectious cysts and motile trophozoites, which replicate within the intestinal lumen. Under conditions that are still poorly understood, the parasite can invade the intestinal mucosa and disseminate via the bloodstream to the liver. The pathogenesis of ALA is driven by a complex interplay between parasite-derived virulence factors and the host immune response.

Shortly after *E. histolytica* invades the liver, a pronounced infiltration of neutrophils and monocytes is observed [2–4]. These recruited cells, together with liver-resident Kupffer cells, play key roles in both early parasite control and tissue damage by rapidly inducing inflammatory mediators such as IL-6, IL-1β, TNF-α, IFN-γ, CXCL1 and CCL2, which promote the recruitment of additional immune cells and amplify the local inflammatory response [4–9]. Beyond their role in acute defence, dysregulated monocyte responses have been identified as critical drivers of hepatic immunopathology. In this context, Sellau *et al.* highlight that both the recruitment and functional polarisation of monocytes and neutrophils are key determinants of whether immune responses remain protective or shift towards tissue-damaging inflammation in the liver [10].

The activation of these innate immune cells is initiated through the recognition of amoebic components by pattern recognition receptors, including Toll-like receptors (TLRs), such as TLR2 and TLR4. Among the hepatic immune cell populations, Kupffer cells play a central role in early parasite sensing and the initiation of

pro-inflammatory signalling [11,12]. However, their activation can also exacerbate liver damage by promoting TNF production, thereby enhancing monocyte- and neutrophil-mediated tissue destruction. Consistently, depletion of Kupffer cells markedly reduces hepatic injury [2].

Neutrophils contribute to host defence against *E. histolytica* through the release of reactive oxygen species (ROS) and proteolytic enzymes, but these mechanisms can also promote collateral host tissue damage [13]. In addition, neutrophils can form neutrophil extracellular traps (NETs) in response to direct parasite contact or parasite-derived components. While NETs may immobilise amoebae, their effectiveness is limited, as *E. histolytica* expresses nucleases capable of degrading them [14–17]. Importantly, NET formation and neutrophil activation have been implicated in immunopathological processes, suggesting that excessive or dysregulated neutrophil responses may contribute to tissue injury rather than protection.

In addition to the host response, the virulence factors of *E. histolytica* play a decisive role in liver pathology. These include the Gal/GalNAc lectin, which mediates adhesion to host mucins in the gut and to host cells during tissue invasion, amoebic pore-forming proteins (amoebapores) that lyse target cells, and a 33-member family of papain-like cysteine peptidases (EhCPs) responsible for tissue degradation [18–22].

Experimental studies further suggest that different *E. histolytica* clones contribute to pathogenesis to varying degrees. Clonal lines derived from the reference strain HM-1:IMSS display substantial differences in virulence; some reliably induce liver abscesses in animal models, while others cause minimal or no lesions [18]. Transcriptomic comparison of the non-pathogenic clone $A1^{np}$ and the pathogenic clone $B2^{p}$ identified 76 differentially expressed genes (46 upregulated in $A1^{np}$ versus $B2^{p}$ and 30 upregulated in $B2^{p}$ versus $A1^{np}$) [18]. Functional assays using overexpression transfectants identified eight proteins that modulate pathogenicity, including a metallopeptidase, C2 domain containing proteins, alcohol dehydrogenases, and several hypothetical proteins [18]. Furthermore, RNA interference approaches were used to analyze the contribution of genes differentially expressed between $A1^{np}$ and $B2^{p}$ trophozoites to pathogenicity. Trigger-induced RNAi-mediated gene silencing of 15 candidates revealed specific effects on ALA formation in a mouse model [23]. Consistent with these differences in pathogenicity, the $B2^{p}$ clone reproducibly induces well-defined amoebic liver abscesses in the established mouse model, whereas $A1^{np}$ infection generally results in substantially smaller and less developed hepatic lesions. This phenotypic difference also provides the basis for using $B2^{p}$-infected tissue for spatial immunohistological characterisation of selected host-response markers [18,23].

However, it remains unclear whether and how the hepatic host response differs in a clone-specific manner between infections with pathogenic and non-pathogenic *E. histolytica* trophozoites. While differences in parasite virulence and selected host responses have been described, a systematic and time-resolved comparison of the global host response, particularly at the transcriptional level, is still lacking.

This study aimed to analyse the temporal dynamics of the hepatic response to infection with non-pathogenic ($A1^{np}$) and pathogenic ($B2^{p}$) *E. histolytica* trophozoites using a murine model. By performing transcriptomic analyses at three time points (6, 12 and 24 hours post infection (hpi)) after intrahepatic infection, we sought to determine how parasite-specific differences shape the hepatic immune profile. The data revealed shared patterns of innate immune activation as well as clone-specific differences in the magnitude, composition and temporal dynamics, highlighting clone-specific modulation of host immunity. While $A1^{np}$ trophozoites triggered a rapid, classical inflammatory response with a strong antimicrobial component, $B2^{p}$ induced a markedly enhanced and complex immune reaction characterised by a combination of pro-inflammatory signalling, cellular stress pathways, and counter-regulatory mechanisms. These findings emphasise that distinct *E. histolytica* clones elicit unique host immune responses, which play a crucial role in determining disease progression and the extent of liver tissue damage.

Methods

Ethics statement

The animal experiments were conducted as part of an earlier doctoral research project under animal-use approval no. 145/13, issued by the competent authority of the State of Hamburg, Germany (Ministry of Health and Consumer

Protection) on 20 January 2014 and conducted in accordance with institutional regulations and the ARRIVE guidelines (https://www.nc3rs.org.uk/arrive-guidelines). All animal procedures reported here were performed during the period covered by this approval and in accordance with the approved experimental protocol. No additional animal experiments were performed for the present study; the current work is based on samples and transcriptomic data generated during the original animal experiments and analysed subsequently for the present study.

E. histolytica cell culture

E. histolytica trophozoites were maintained axenically under microaerophilic conditions at 37°C in TYI-S-33 medium [24] using plastic culture flasks (Corning, Kaiserslautern, Germany). Non-pathogenic clone A1^{np} and pathogenic clone B2^{p} originated from the HM-1:IMSS-A and HM-1:IMSS-B cell lines, respectively [18].

ALA formation in mice

Animal infections were performed with 10- to 12-week-old male C57BL/6 mice bred in the animal facility of the Bernhard Nocht Institute for Tropical Medicine (Hamburg, Germany).

For infection experiments, 1×10^6 *E. histolytica* trophozoites were cultured in 75 ml culture flasks for 24 hours. After incubation, the cells were harvested and resuspended in incomplete TYI-S-33 medium. Then, 1.25×10^5 trophozoites in 25 µl of incomplete TYI-S-33 medium were injected directly into the left liver lobe as previously described [4,18]. The mice were sacrificed at 6, 12 and 24 hpi, after which the infected liver lobe was transferred either into TRIzol reagent (Thermo Fisher Scientific) for RNA extraction or fixed in 4% formalin for immunohistochemistry.

For each time point and each *E. histolytica* clone (A1^{np} and B2^{p}), liver samples from four individual mice were analysed as independent biological replicates (n = 4 per clone and time point). The untreated control group consisted of five individual mice (n = 5). Samples were analysed individually and were not pooled.

Since no sham-injected control group was included, all control comparisons were made against untreated animals. To account for potential procedure-related effects, particular emphasis was placed on the direct comparison between A1^{np} and B2^{p} infections.

RNA extraction and RNAseq

The liver tissue was homogenised in 500 µL of TRIzol reagent (Thermo Fisher Scientific). An additional 500 µL of TRIzol was added after homogenisation. RNA was then isolated using the mirVana miRNA Isolation Kit (Ambion), following the manufacturer's protocol.

RNA concentration and integrity were assessed spectrophotometrically using a NanoDrop 2000 (Thermo Fisher Scientific) and with an Agilent 2100 Bioanalyzer employing the RNA 6000 Pico Assay kit (Agilent Technologies). Potential genomic DNA contamination was eliminated using the TURBO DNA-free Kit (Thermo Fisher Scientific, Hampton, NH, USA). Library preparation and high-throughput RNA sequencing were conducted by BGI (Shenzhen, China) using the Illumina HiSeq 4000 platform with paired-end 100 bp reads (PE100).

Bioinformatic Analyses/Statistics

RNA-seq data was processed using CLC Genomics Workbench v24.0 (QIAGEN). Initially, raw sequencing reads were adapter-trimmed and quality-filtered with a quality score of 0.05. Reads were subsequently mapped to the *Mus musculus* reference genome (GRCm39), and gene expression was quantified in Transcripts Per Million (TPM). Differential gene expression was analyzed using the "Differential Expression for RNA-Seq" tool implemented in CLC Genomics Workbench, which models RNA-seq read counts using a negative binomial generalized linear model (GLM). Pairwise differences between experimental groups were assessed using Wald tests, and *p* values were adjusted for multiple testing using the

Benjamini–Hochberg false discovery rate (FDR) procedure. Genes were considered differentially expressed when they showed an absolute fold change of ≥ 2.0, an FDR-adjusted *p* value of ≤ 0.05, and a minimum TPM threshold of ≥ 2.0. Heatmaps were created using the R/Shiny-based tool Heatmapper [25]. The interaction network analysis was performed with the database STRING, version 12.0 [26]. The following setting was used: Active interaction sources: text mining, experiments, databases, co-expression; Meaning of network edges: high confidence 0.700; Network display mode: Interactive; Network display options: Hide disconnected nodes in the network; Clustering Options: MCL clustering, inflation parameter 3. Visualization of functional enrichment for Reactome and KEGG pathways was performed using STRING. Volcano plots for the visualization of significantly differentially expressed genes were created using the European Galaxy Server (https://rna.usegalaxy.eu/) [27].

Immunohistology

Liver tissue from mice infected with pathogenic B2^{p} trophozoites was fixed in formalin (4%) and embedded in paraffin. Sections (0.2 mm) were stained with H&E (Hematoxylin and Eosin), or prepared for immunohistochemistry. Immunohistochemistry was performed using the following primary antibodies: anti-Ackr2 (1:400, Proteintech), anti-Rgs16 (1:400, Biorbyt), anti-Btg2 (1:400, Biorbyt), anti-Gadd45b (1:200, MyBioSource) and anti-Sesn1 (1:400, Biorbyt). Detection was carried out with the Zytomed Chem-Plus HRP Polymer Kit (Zytomed) following the manufacturer's instructions, and visualisation was achieved using 3,3′-diaminobenzidine substrate solution (Dako). Immunohistological analyses were restricted to liver tissue from B2^{p}-infected mice. Infection with the non-pathogenic A1^{np} clone typically results in very small or poorly developed hepatic lesions, which do not consistently provide sufficient lesion architecture for reliable spatial localization analyses. In contrast, B2^{p} infection produces well-defined amoebic liver abscesses, allowing the spatial distribution of selected immune and stress-response proteins to be assessed within the lesion. As this analysis was intended as a spatial validation of selected transcriptomic findings rather than as a quantitative comparison between A1^{np} and B2^{p} infections, no additional animals were used solely to obtain A1^{np} lesion material.

Results

Temporal divergence of hepatic responses to A1^{np} and B2^{p} infection

To define clone-dependent differences in the hepatic host response, A1^{np}- and B2^{p}-infected mice were directly compared across time. Because both infection groups underwent the same intrahepatic injection procedure, the direct A1^{np}-versus-B2^{p} comparison was used as the primary analysis for identifying clone-dependent responses. Comparisons of each infected group with untreated controls were additionally used to describe the overall magnitude and temporal dynamics of the hepatic response. However, in the absence of a sham-injected control group, these latter comparisons may include procedure-related transcriptional effects and are therefore interpreted as infection-associated rather than strictly parasite-specific responses.

Direct comparison of A1^{np}- and B2^{p}-infected livers revealed only 12 differentially expressed genes at 6 hpi, indicating that the early hepatic responses to the two clones were still highly similar. The number of differentially expressed genes between the two infection groups increased markedly to 543 at 12 hpi and 836 at 24 hpi (Fig 1; S1 Table), demonstrating a progressive divergence of the hepatic response over time.

While the direct A1^{np}-versus-B2^{p} comparison provides the most stringent basis for identifying clone-dependent transcriptional differences, it does not fully describe the response pattern elicited by each infection condition. Genes can, for example, show the same direction of regulation in both infection groups but differ in the magnitude of their response relative to baseline without reaching statistical significance in the direct clone-to-clone comparison. We therefore additionally compared each infected group with untreated controls to characterise which genes and pathways were induced or repressed relative to the uninfected state and to place the direct clone-to-clone differences into their biological and

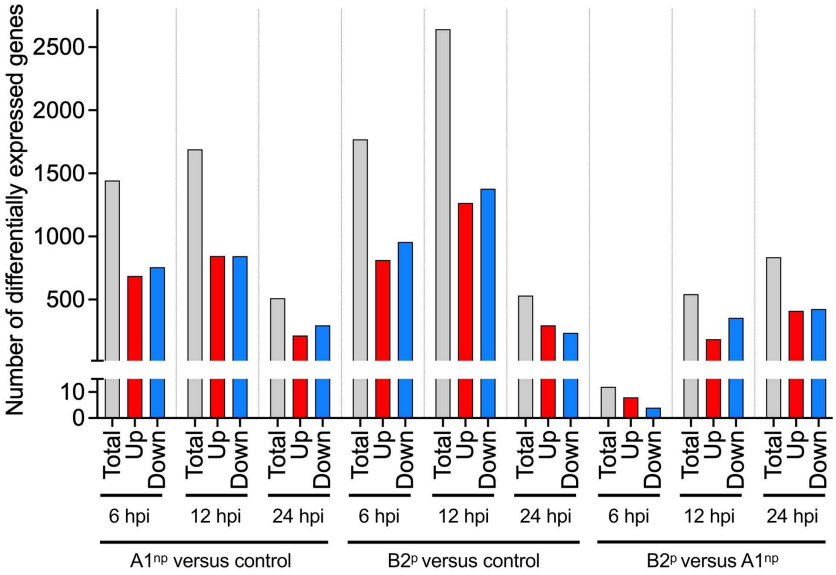


Fig 1. Differential gene expression in liver tissue following infection with A1^{np} and B2^{p} trophozoites. The number of differentially expressed genes (DEGs) in liver tissue of mice intrahepatically infected with *Entamoeba histolytica* clones A1^{np} and B2^{p} is shown at 6, 12, and 24 hours post-infection (hpi). Differential expression analysis was performed relative to uninfected control mice (A1^{np} versus control; B2^{p} versus control) and between infections (B2^{p} versus A1^{np}). Bars represent the total number of DEGs (grey), as well as upregulated (red) and downregulated (blue) genes. Differential expression was defined as ≥2-fold change with FDR < 0.05 (control: n = 5; infected groups: n = 4 per time point).

https://doi.org/10.1371/journal.pntd.0014869.g001

temporal context. These control-based comparisons were not used to infer statistically significant differences between A1^{np} and B2^{p}. Thus, a gene being significantly regulated in B2^{p} versus untreated controls but not in A1^{np} versus untreated controls was interpreted as a more readily detectable response relative to baseline in the B2^{p} condition, but not, by itself, as evidence of a significant difference between the two infection groups.

Using these control-relative comparisons, A1^{np} infection was associated with 687 upregulated and 814 downregulated genes at 6 hpi, whereas B2^{p} infection was associated with 814 upregulated and 952 downregulated genes.At 12 hpi, the total number of differentially expressed genes increased from 1,501–1,689 in the A1^{np} group and from 1,766–2,643 in the B2^{p} group. After 24 hpi, the number of differentially expressed genes decreased considerably. In the A1^{np} group, 215 genes were upregulated and 127 were downregulated, making a total of 342 genes. In the B2^{p} group, 296 genes were upregulated and 236 were found to be downregulated, making a total of 532 genes (Fig 1; S1 Table). Direct comparison of differential gene expression between A1^{np} and B2^{p} revealed only 12 genes at 6 hpi, but this number increased markedly to 543 genes at 12 hpi and further to 836 genes at 24 hpi (Fig 1; S1 Table). Because these comparisons are relative to untreated rather than sham-injected mice, the corresponding DEG counts describe the overall response associated with each infection condition and may include effects of the intrahepatic injection procedure.

When each infection group was compared separately with untreated controls, Reactome and KEGG enrichment analyses of significantly upregulated genes revealed a rapid and pronounced hepatic response already at 6 hpi (Figs 2A and 2B).

In both A1^{np} and B2^{p} infections, KEGG analysis revealed enrichment of central signalling pathways, including MAPK, TNF, NF-κB, FoxO, PPAR and IL-17 signalling, indicating activation of core inflammatory and regulatory networks (Fig 2A). Reactome analysis likewise showed enrichment of pathways related to Toll-like receptor (TLR) signalling, cytokine and interleukin signalling, platelet activation and degranulation, as well as metabolic processes (Fig 2B). These

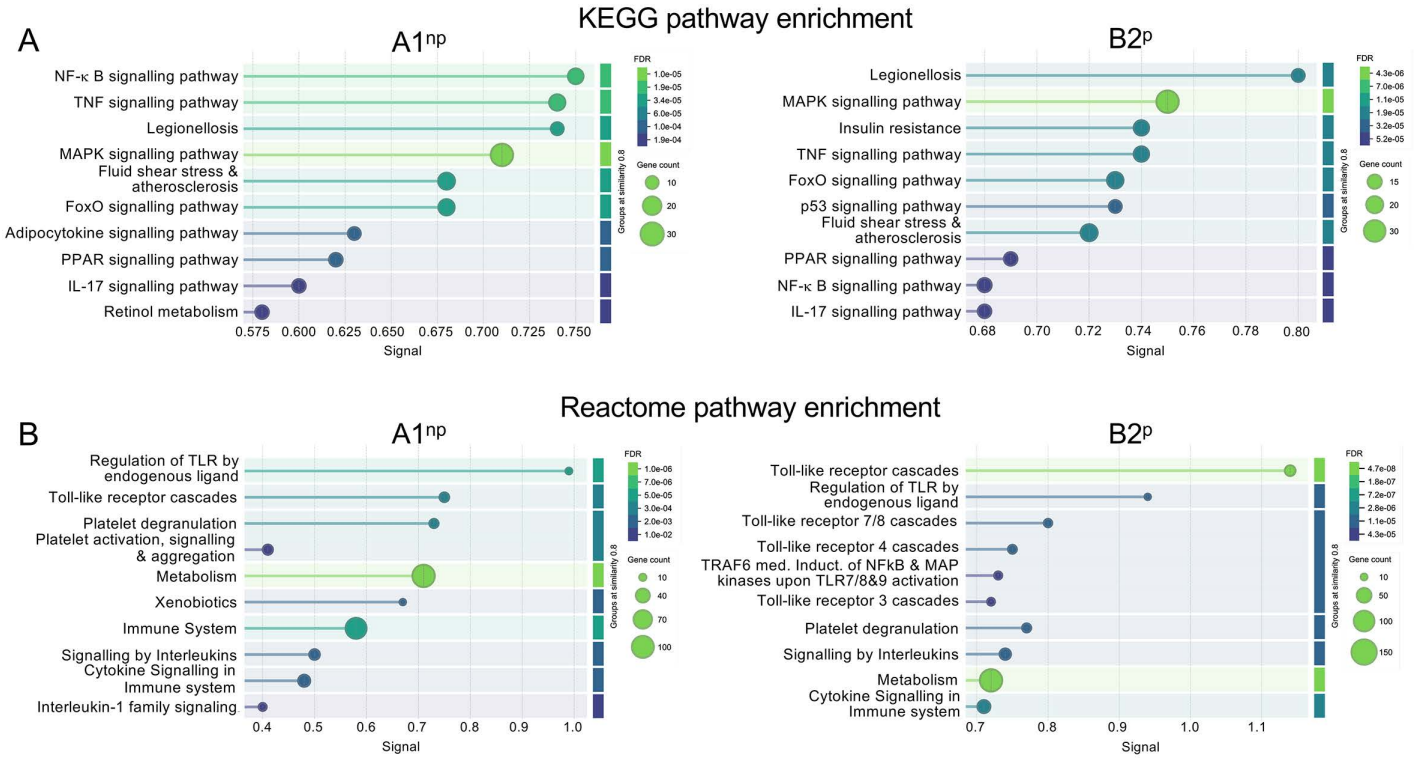


Fig 2. KEGG and Reactome pathway enrichment analysis of genes upregulated at 6 hpi in mice infected with non-pathogenic (A1^{np}) and pathogenic (B2^{p}) *E. histolytica* trophozoites compared to uninfected controls. KEGG (A) and Reactome (B) pathway enrichment analysis was performed using all genes that were significantly upregulated at 6 hpi in mouse liver tissue in comparison to the uninfected control (fold change (FC) ≥ 2.0; false discovery rate (FDR) < 0.05). The pathways are shown for the non-pathogenic clone A1^{np} (left panels) and the pathogenic clone B2^{p} (right panels). The x-axis represents the enrichment signal, reflecting the strength of pathway overrepresentation. Dot size indicates the number of genes associated with each pathway (gene count), and the colour gradient represents the FDR-adjusted *p*-value. Control: n = 5; A1^{np} and B2^{p}: n = 4.

https://doi.org/10.1371/journal.pntd.0014869.g002

analyses describe pathway patterns within each infection condition relative to untreated controls; they do not by themselves constitute a statistical test of pathway differences between A1^{np} and B2^{p} infections.

Within these control-relative enrichment profiles at 6 hpi, A1^{np}-infected livers showed enrichment of pathways related to retinol metabolism and adipocytokine signalling, in addition to cytokine- and interleukin-associated pathways (Fig 2A and 2B). The B2^{p} control-relative profile included multiple Toll-like receptor cascades as well as insulin and p53 signalling pathways (Fig 2A and 2B). These differences in enrichment profiles are descriptive and should be interpreted cautiously, particularly because the direct A1^{np}-versus-B2^{p} comparison identified only 12 differentially expressed genes at this early time point. Formal clone-dependent differences were therefore assessed using the direct comparison between the two infection groups, as described below.

At 12 hpi, the direct differential expression analysis demonstrated substantially greater divergence between A1^{np}- and B2^{p}-infected livers (543 differentially expressed genes; Fig 1; S1 Table). In the separate comparisons with untreated controls, only three KEGG pathways were enriched in both infection groups: IL-17 signalling, AGE-RAGE signalling in diabetic complications, and TNF signalling pathways (Fig 3A). Reactome analysis likewise identified shared Toll-like receptor cascades, and general immune-system pathways (Fig 3B).

Among pathways enriched relative to untreated controls at 12 hpi, the A1^{np} profile included cytokine-cytokine receptor interaction, PPAR signalling pathway, viral protein interaction with cytokine and cytokine receptor, complement and

coagulation cascades, NF-κB signalling pathway and rheumatoid arthritis (Fig 3A). Disease-specific KEGG pathway names such as “rheumatoid arthritis”, “Legionellosis” or “Chagas disease” reflect overlap with shared innate immune and inflammatory gene modules and should not be interpreted as evidence of these diseases or co-morbidities in the present model. Reactome analysis of the A1^{np}-versus-control comparison additionally identified platelet degranulation, pathways of fibrin clot formation, metabolism of lipids and metabolism (Fig 3B). These findings describe the biological processes represented in the A1^{np}-associated response relative to untreated controls but are not interpreted as evidence that these pathways are significantly different from B2^{p} infection.

In the B2^{p}-versus-control comparison at 12 hpi, enriched KEGG pathways included FoxO, MAPK and p53 signalling (Fig 3A), while Reactome analysis identified TLR3- and TLR4-associated cascades and downstream TRAF6- and the MyD88/MAL-dependent signalling axes (Fig 3B). Thus, the control-relative B2^{p} profile contained multiple pathways associated with inflammatory and cellular stress responses. As above, differences between the two control-relative enrichment profiles are considered descriptive; clone-dependent effects are inferred primarily from the direct A1^{np}-versus-B2^{p} differential expression analysis.

At 24 hpi, the direct comparison revealed the largest divergence between the two infection groups, with 836 differentially expressed genes (Fig 1; S1 Table).

In the separate comparisons with untreated controls, both infection conditions showed enrichment of several shared KEGG pathways, including IL-17 signalling pathway, viral protein interaction with cytokine and cytokine receptors, retinol

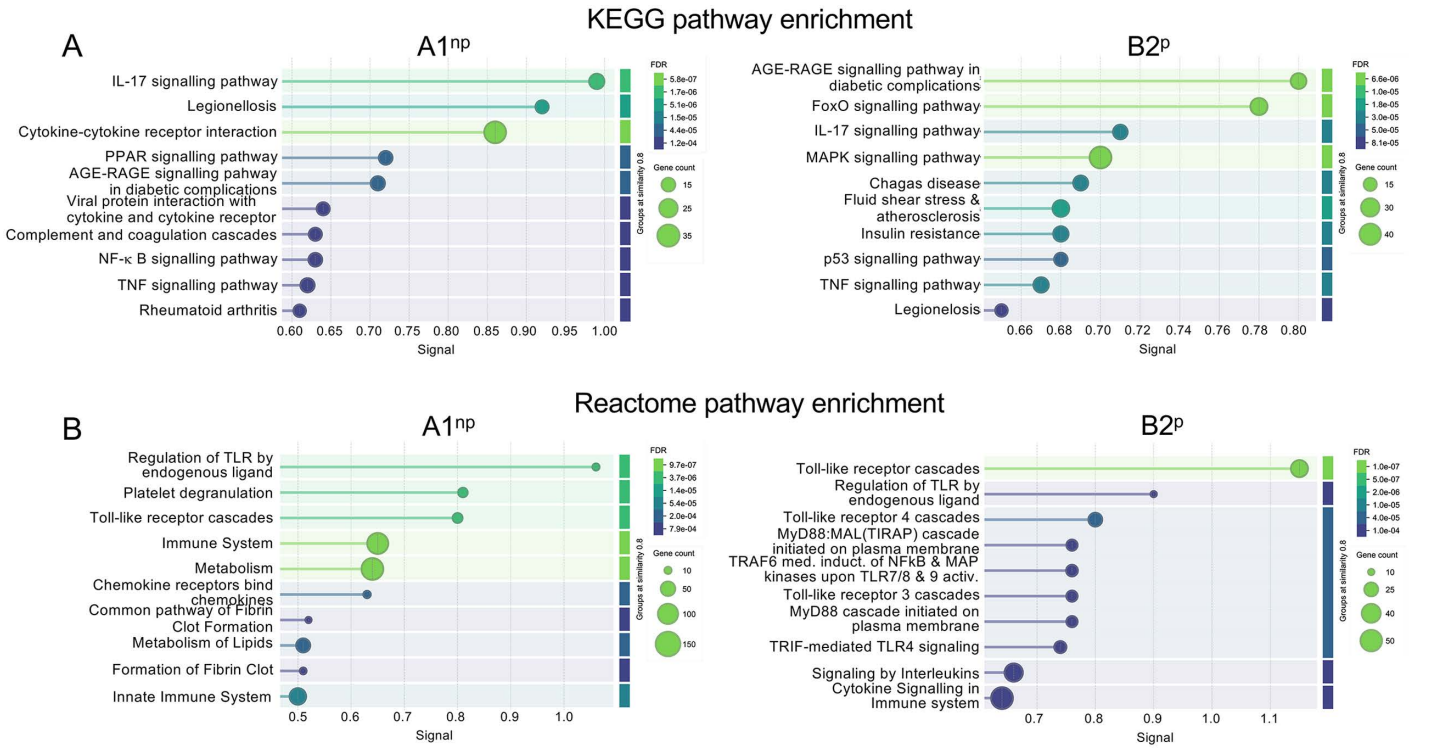


Fig 3. KEGG and Reactome pathway enrichment analysis of genes upregulated at 12 hpi in mice infected with non-pathogenic (A1^{np}) and pathogenic (B2^{p}) *E. histolytica* trophozoites compared to uninfected controls. KEGG (A) and Reactome (B) pathway enrichment analysis was performed using all genes that were significantly upregulated at 12 hpi in mouse liver tissue in comparison to the uninfected control (FC ≥ 2.0; FDR ≤ 0.05). The pathways are presented for the non-pathogenic clone A1^{np} (left panels) and the pathogenic clone B2^{p} (right panels). The x-axis represents the enrichment signal, reflecting the strength of pathway overrepresentation. Dot size indicates the number of genes associated with each pathway (gene count), and the colour gradient represents the adjusted *p*-value (FDR). Control: n = 5; A1^{np} and B2^{p}: n = 4.

https://doi.org/10.1371/journal.pntd.0014869.g003

metabolism, and legionellosis, (Fig 4A), while additional pathways differed between the two control-relative enrichment profiles.

In the A1^{np}-versus-control comparison at 24 hpi, enriched KEGG pathways included arachidonic acid metabolism, steroid hormone biosynthesis, and linoleic acid metabolism. The B2p-versus-control comparison showed enrichment of pathways including cytokine–cytokine receptor interaction, NF-κB signalling, rheumatoid arthritis, PPAR signalling, complement and coagulation cascades, and hematopoietic cell lineage (Fig 4A). Reactome analysis identified several pathways in both control-relative profiles, including platelet degranulation, regulation of Toll-like receptor (TLR) signalling by endogenous ligands, the immune system, neutrophil degranulation, and hemostasis. Additional pathways in the A1^{np} profile included metal sequestration by antimicrobial proteins, cytochrome P450, phase I functionalization of compounds, and steroid metabolism, whereas the B2^{p} profile included chemokine receptors, chemokine-binding receptors, and peptide ligand-binding receptors (Fig 4B). These results illustrate differences in the composition of the two control-relative enrichment profiles, but direct clone-to-clone analyses were used to establish clone-dependent transcriptional differences.

Immune-related gene expression patterns during A1^{np} and B2^{p} infection

Taken together, the pathway analyses relative to untreated controls characterise the broad biological programmes associated with each infection condition, but they cannot by themselves distinguish parasite-induced responses from

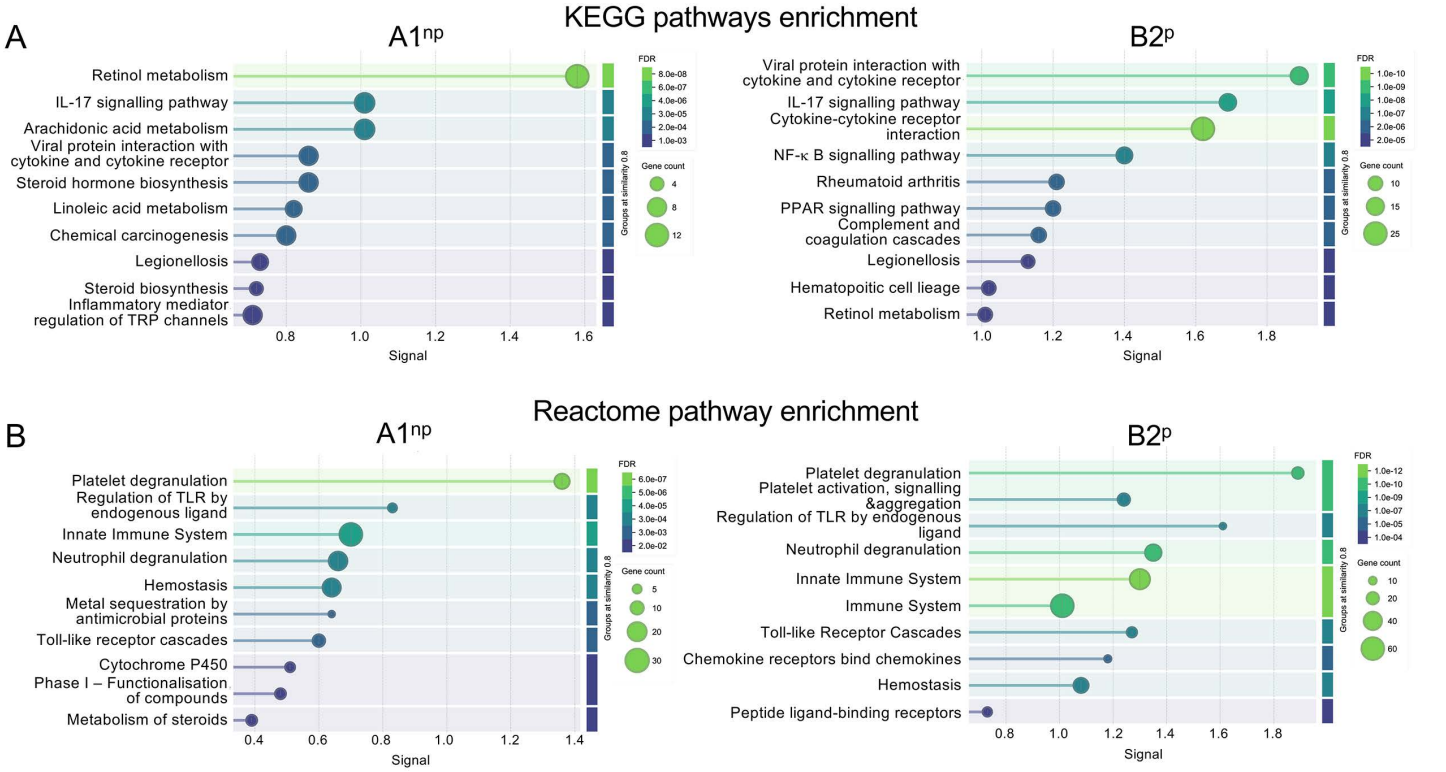


Fig 4. KEGG and Reactome pathway enrichment analysis of genes upregulated at 24 hpi in mice infected with non-pathogenic (A1^{np}) and pathogenic (B2^{p}) *E. histolytica* trophozoites compared to uninfected controls. KEGG (A) and Reactome (B) pathway enrichment analysis was performed using all genes that were significantly upregulated at 24 hpi in mouse liver tissue in comparison to the uninfected control (FC ≥ 2.0; FDR ≤ 0.05). The pathways are presented for the non-pathogenic clone A1^{np} (left panels) and the pathogenic clone B2^{p} (right panels). The x-axis represents the enrichment signal, reflecting the strength of pathway overrepresentation. Dot size indicates the number of genes associated with each pathway (gene count), and the colour gradient represents the adjusted *p*-value (FDR). Control: n = 5; A1^{np} and B2^{p}: n = 4.

https://doi.org/10.1371/journal.pntd.0014869.g004

effects of the intrahepatic procedure or formally establish pathway differences between the two clones. Accordingly, clone-dependent conclusions in this study are based primarily on the direct A1^{np}-versus-B2^{p} comparison. To examine the immune component of the response in more detail, we next inspected the expression of 151 genes linked to immune pathways that were regulated in the infection-versus-control datasets (S3 Table). Most of these genes were upregulated in both infection groups.

Although distinct expression patterns also emerged over time, several genes were similarly regulated in response to both A1^{np} and B2^{p} trophozoites over the course of infection. At 6 hpi, shared transcriptional responses included the significant upregulation of genes involved in sensing and regulating the innate immune response. These genes included *Clec4e*, *Cd14*, *Irak3*, *Cd33*, and *Cd300lf* (Fig 5B, S3 Table). Several inflammation- and metabolism-associated genes were also co-regulated, including *Cxcl2*, *Acod1*, *Serpina3g*/*n*/*m* and *Slfn4*, all of which showed similarly high fold changes in both groups (Figs 5A-5C, S3 Table).

At 12 hpi, a subset of these genes remained commonly upregulated, such as *Il1rn*, *Cxcl1*, *Cxcr4*, *C5ar1*, *Csf3r*, and again *Serpina3m*, indicating a sustained inflammatory and regulatory response in both infection settings (Figs 5A and 5B; S3 Table).

Further overlap in gene regulation was observed between the two groups by 24 hpi, including for *Cxcr4, Csf3r*, *Hp*, *Itgam*, *Cish*, *Cd33*, and *Gas6* (Figs 5A and 5B, S3 Table).

Despite these shared responses, the direct A1^{np}-versus-B2^{p} analysis demonstrated that transcriptional divergence increased strongly over time, from only 12 differentially expressed genes at 6 hpi to 543 at 12 hpi and 836 at 24 hpi (Fig 1; S1 Table). The following gene-level descriptions illustrate expression patterns within the immune-related gene set (Fig 5); formal statistical identification of clone-dependent differentially expressed genes is presented in the direct comparison below (Fig 7).

As early as 6 hpi, distinct differences in gene expression emerged between the two infection groups, with several genes being more strongly upregulated following B2^{p} infection. These included *Il1r2*, *Rgs16*, *Cxcl3*, *Gadd45b*, *Gadd45g*, *Txnip*, *Mmp8*, *Osm* and *Igfbp1*. In contrast, stronger expression in the A1^{np} group was observed for *Serpine1*, *Lcn2*, and *Cxcl1* (Fig 5A, S3 Table).

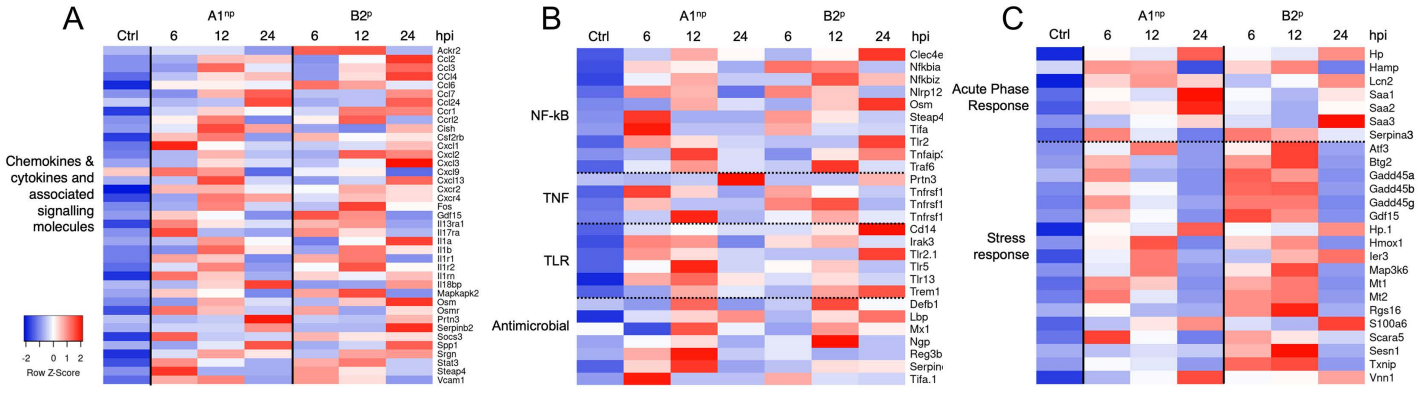


Fig 5. Time-resolved hepatic gene expression responses to infection with A1^{np} and B2^{p} trophozoites. (A-C) Heatmaps showing the average expression of selected genes in liver tissue at 6, 12, and 24 hpi infected either with non-pathogenic (A1^{p}) or pathogenic (B2^{p}) *E. histolytica* trophozoites (n = 4). Expression values are shown as Z-scores for each row, calculated from normalised TPMs (transcripts per million). Red indicates high gene expression and blue indicates low gene expression (ctrl; uninfected mice, n = 5). Genes are grouped according to functional categories: (A) chemokines, cytokines, and associated signalling molecules; (B) key inflammatory pathways including NF-κB, TNF, TLR signalling, and antimicrobial responses; (C) acute phase and stress response genes.

https://doi.org/10.1371/journal.pntd.0014869.g005

At 12 hpi, the expression of genes encoding chemokines and their receptors was again more pronounced in the B2^{p} group, including *Cxcl2*, *Ccr1*, and *Cxcr2*. In contrast, *Ccl7* and *Cxcl3* showed slightly higher expression in the A1^{np} group (Fig 5A, S3 Table). *Ackr2*, which encodes an atypical chemokine receptor involved in chemokine degradation, was also induced more strongly following B2^{p} infection (Fig 5A, S3 Table). Genes involved in interleukin signalling exhibited a consistent trend towards higher expression in the B2^{p} group, including *Il1b*, *Il1r1*, *Il17ra*, and *Il1r2* while *Il1rn* was similarly expressed in both groups (Fig 5A, S3 Table). The expression of genes involved in signal transduction pathways was also more strongly induced by B2^{p} infection. These genes included *Nfkbia*, *Ripk*, *Traf6*, and *Socs2* (Fig 5B, S3 Table). Additional genes associated with T cell regulation and inflammation, such as *Tnfrsf1b*, *Phf11*, and *Rgs16*, were also more strongly expressed in the B2^{p} group (Figs 5B and 5C, S3 Table). Similarly, genes associated with the stress response and redox including *Gadd45a*, *Gadd45b*, *Gadd45g*, *Txnip*, *Mt1*, and *Mt2* were also upregulated to a greater extent in the B2^{p} group (Fig 5C, S3 Table). In terms of antimicrobial responses, *Reg3b* showed a significant increase following A1^{np} infection, whereas *Ngp*, a neutrophil-specific antimicrobial protein, exhibited stronger induction in the B2^{p} group (Fig 5B, S3 Table).

This pattern of heightened gene expression in the B2^{p} group persisted at 24 hpi. There was stronger induction for *Cxcl3*, *Cxcl2*, *Ccl3*, *Osm*, *Il1r2*, and *Trem1*. Additionally, pro-inflammatory and innate immunity-related genes, including *Ptgs2*, *Saa3*, *Clec4d*, *Clec4e*, and *Serpine1* exhibited higher expression following B2^{p} infection. An exception to this trend was *Saa2*, which exhibited higher expression in the A1^{np} group (Figs 5A-5C; S3 Table).

Temporal progression of inflammatory networks

Fig 6 shows the temporal development of gene expression (fold change compared to untreated control) of a STRING cluster containing genes associated with neutrophil chemotaxis, the interaction of viral proteins with cytokines and cytokine receptors, and the inflammatory response. This visualization is descriptive and compares the magnitude of control-relative fold changes between the two infection conditions; it is not used as a substitute for direct differential expression testing between A1^{np} and B2^{p}.

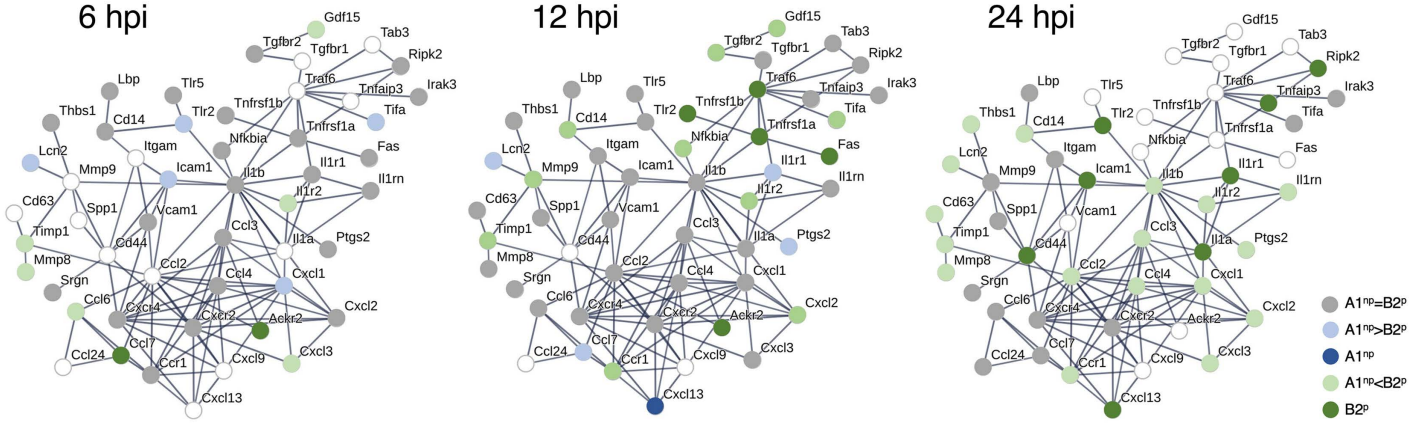


Fig 6. STRING cluster of neutrophil chemotaxis and cytokine signalling. The STRING cluster comprises genes associated with neutrophil chemotaxis, cytokine signalling and inflammatory responses. Temporal regulation at 6, 12 and 24 hpi is shown. Genes that do not exhibit differential expression during infection with A1^{np} or B2^{p} trophozoites in comparison to the control are represented as unfilled circles. Genes with similar differential expression after A1^{np} and B2^{p} infection are shown as grey circles (FC < 2.0). Those more strongly expressed after A1^{np} infection than B2^{p} infection are shown in light blue. Genes that are more strongly expressed after B2^{p} infection than after A1^{np} infection are shown in light green Genes that are exclusively expressed following infection by one clone only are marked in dark blue for A1^{np} trophozoites and in dark green for B2^{p} trophozoites.

https://doi.org/10.1371/journal.pntd.0014869.g006

To simplify the presentation, Fig 6 provides a categorical representation of the expression data (S1 Table), indicating whether a gene is similarly regulated in both infections (grey), is more strongly upregulated after $A1^{np}$ infection (light blue), or after $B2^{p}$ infection (light green). Genes that are expressed exclusively after infection with one clone are marked in dark blue ($A1^{np}$) or dark green ($B2^{p}$). After 6 hpi, 23 genes show comparable regulation in both infection groups, while seven genes in the $B2^{p}$ group show higher control-relative fold changes than in the $A1^{np}$ group and five genes show higher fold changes after $A1^{np}$ infection. At 12 hpi, 27 genes remain similarly regulated, but 15 genes show higher control-relative fold changes in the $B2^{p}$ group, compared with five in the $A1^{np}$ group. At 24 hpi, the number of genes with similar regulation drops to 12, while 24 genes are higher control-relative fold changes after $B2^{p}$ infection. At this point, no gene in this cluster shows a higher control-relative fold change in the $A1^{np}$ group.

Time-dependent differences in biological processes between $A1^{np}$ and $B2^{p}$ infections

To formally identify clone-dependent transcriptional differences while controlling for the shared intrahepatic injection procedure, we performed direct differential expression analysis between $B2^{p}$- and $A1^{np}$-infected livers. At 6 hpi, only eight genes were upregulated in liver cells following $B2^{p}$ infection compared to $A1^{np}$, whereas four genes were downregulated. By 12 hpi, this number had increased markedly, with 187 genes upregulated and 356 genes downregulated in the $B2^{p}$-versus-$A1^{np}$ comparison. At 24 hpi, 411 genes were upregulated and 425 were downregulated in $B2^{p}$-infected mice relative to $A1^{np}$-infected mice (Fig 1, Figs 7A-7C, S1 Table). This direct comparison constitutes the primary basis for conclusions regarding clone-dependent host responses.

Functional enrichment of genes identified in the direct $B2^{p}$-versus-$A1^{np}$ comparison revealed distinct biological processes at 12 and 24 hpi (Figs 7D-7G).

At 12 hpi, genes that were upregulated in $B2^{p}$-infected mice relative to $A1^{np}$-infected mice were enriched in pathways related to cellular responses to oxygen-containing compounds, hormones, peptides and lipids (Fig 7D). Conversely, genes that were upregulated in $A1^{np}$- relative to $B2^{p}$-infected mice were associated with the regulation of metabolic processes, including primary and cellular metabolism, as well as DNA catabolic processes and cellular responses to DNA damage (Fig 7E).

At 24 hpi, genes that were upregulated in $B2^{p}$- relative to $A1^{np}$-infected mice were predominantly enriched in pathways related to the biosynthesis and metabolism of steroids, sterols, and cholesterol (Fig 7F). Conversely, genes that were upregulated in $A1^{np}$-infected mice relative to $B2^{p}$-infected mice were associated with triglyceride and acylglycerol metabolic processes, small molecule metabolism, and responses to hormonal stimuli (Fig 7G). Together, these data demonstrate time-dependent differences in the biological processes associated with differentially expressed genes in $A1^{np}$ and $B2^{p}$ infections.

Validation of gene expression at the protein level reveals distinct expression and localization of immune regulators in amoebic liver abscesses

To further examine selected genes associated with inflammatory regulation and cellular stress, transcript levels of *Ackr2, Btg2, Gadd45b, Rgs16* and *Sesn1* were analysed individually over the course of infection (Fig 8). All five genes showed time-dependent induction following infection, with a generally more pronounced response in $B2^{p}$-infected livers. *Ackr2* expression was elevated particularly at 6 and 12 hpi after $B2^{p}$ infection, whereas *Btg2* showed a marked increase at 12 hpi. Similarly, *Gadd45b* and *Rgs16* displayed strong early-to-intermediate induction following $B2^{p}$ infection, with higher transcript levels than in untreated controls and, at several time points, than in $A1^{np}$-infected livers. *Sesn1* also showed its strongest increase at 12 hpi in the $B2^{p}$ group. Together, these expression profiles support the broader transcriptomic finding that pathogenic $B2^{p}$ infection is associated with enhanced activation of genes involved in inflammatory regulation, signal transduction and cellular stress responses.

Based on these transcriptional patterns, the corresponding proteins were subsequently analysed by immunohistochemistry to assess their spatial distribution within amoebic liver abscesses. Cells positive for *Ackr2*, *Btg2* and *Sesn1* accumulated

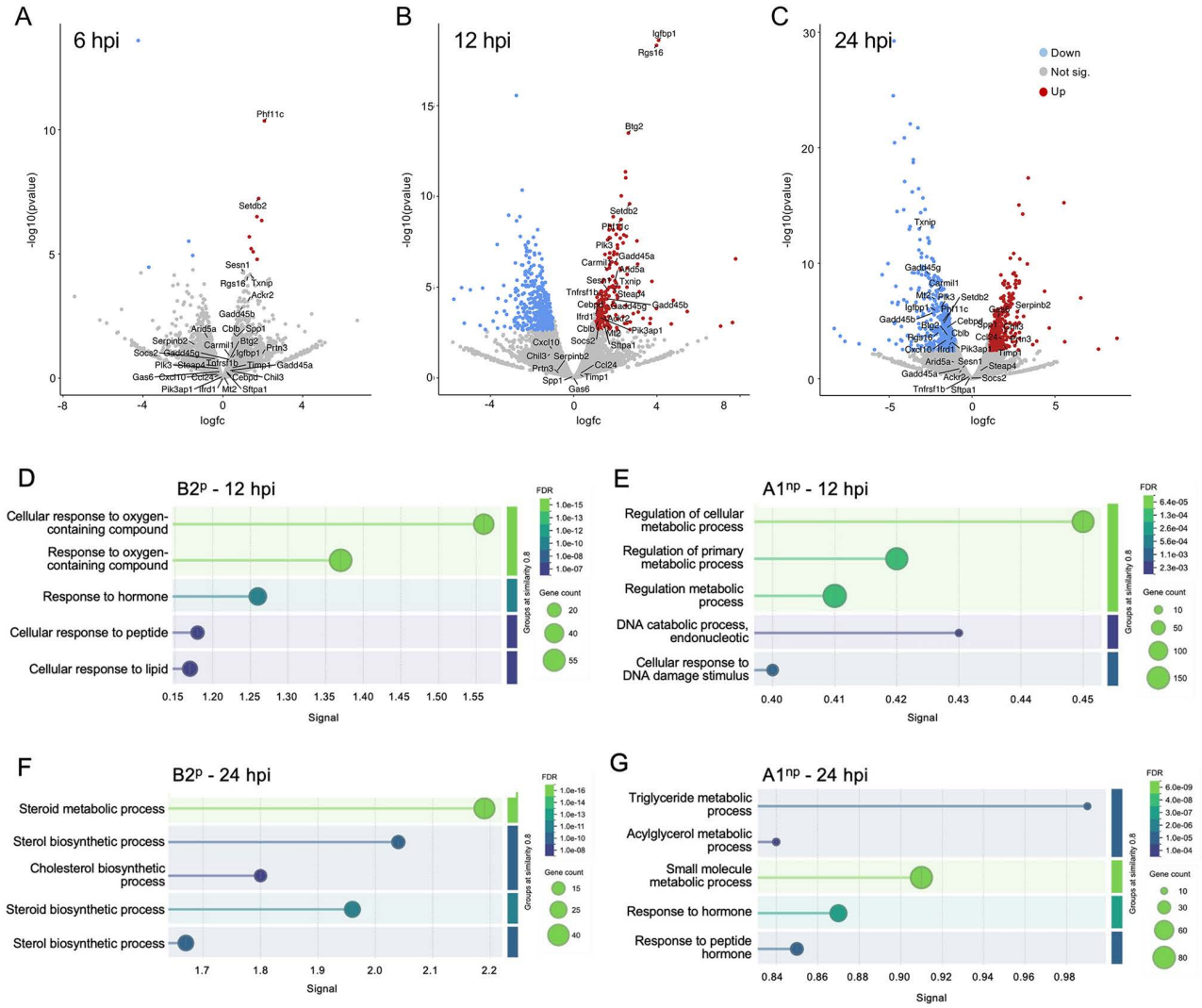


Fig 7. Differential gene expression and enrichment of biological processes in liver tissue following infection with A1^{np} and B2^{p} trophozoites. (A–C) Volcano plots showing differentially expressed genes (FC ≥ 2, FDR < 0.05) in liver cells at 6 (A), 12 (B) and 24 (C) hpi in the direct comparison between B2^{p}- and A1^{np}-infected mice. Each dot represents one gene, plotted according to log fold change (logFC) versus –log$_{10}$(p-value). Significantly upregulated genes in B2^{p} compared to A1^{np} are shown in red, downregulated genes in blue and non-significantly regulated genes in grey. (D–G) Gene ontology (GO) term biological processes enriched in genes that were differentially expressed between A1^{np}-and B2^{p}-infected mice at 12 and 24 hpi. The left panels (D, F) show significantly enriched GO biological process terms for genes that are upregulated in B2^{p}-infected mice relative to A1^{np}-infected mice, and the right panels show the same for genes that are upregulated in A1^{np}-infected mice relative to B2^{p}-infected mice (E, G). The data are presented separately for 12 hpi (upper panels, D, E) and 24 hpi (lower panels, F, G).

https://doi.org/10.1371/journal.pntd.0014869.g007

predominantly at the margin of the ALA, whereas Gadd45b- and Rgs16-positive cells were more frequently detected within the central regions of the ALA, in closer proximity to the trophozoites(Fig 9). These findings demonstrate distinct spatial expression patterns of the selected immune- and stress-associated proteins within B2^{p}-induced liver lesions.

Discussion

This study provides detailed insights into how two clones of *Entamoeba histolytica*, which differ in their pathogenicity, modulate the hepatic immune response. By comparing the transcriptional profiles of non-pathogenic A1^{np} and pathogenic

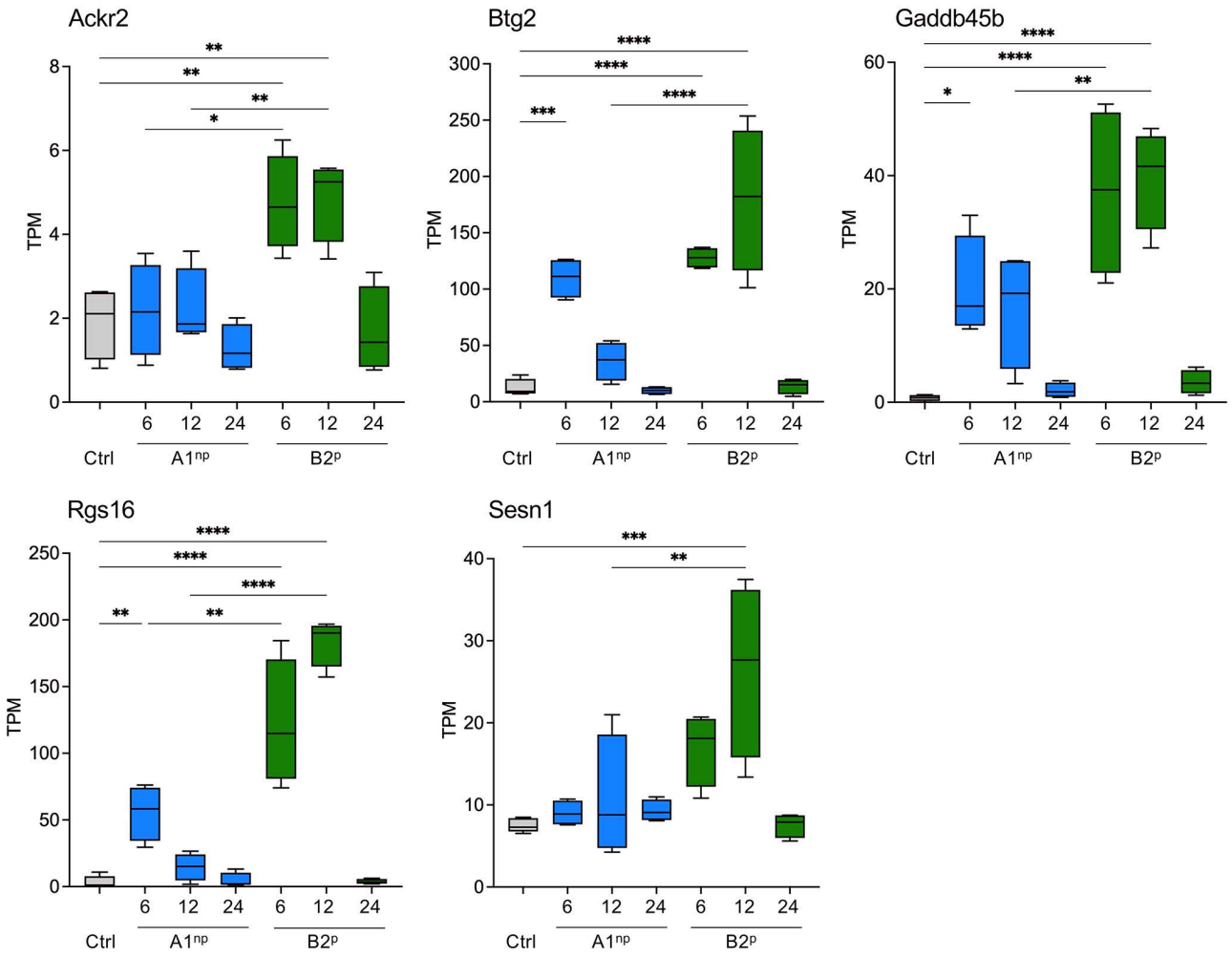


Fig 8. | Time-dependent regulation of selected stress and immune response genes in the liver after infection with *Entamoeba histolytica*. Box plots show the transcript amounts (TPM) of *Ackr2*, *Btg2*, *Gadd45b*, *Rgs16* and *Sesn1* in liver tissue of untreated control animals (Ctrl, n = 5) and 6, 12 and 24 hours after intrahepatic infection with the non-pathogenic clone A1^{np} (blue, n = 4) or the pathogenic clone B2^{p} (green, n = 4). The data illustrate a pronounced, temporally differentiated gene induction, especially after B2^{p} infection, with strong activation of stress- and signal transduction-associated genes. Boxes represent median and interquartile range; whiskers represent minimum and maximum values. Statistical significance between groups is indicated by asterisks (* $p < 0.05$; ** $p < 0.01$; *** $p < 0.001$; **** $p < 0.0001$).

https://doi.org/10.1371/journal.pntd.0014869.g008

B2^{p} trophozoites over time, we identified regulatory patterns that are both shared and distinct, and which shape the magnitude, composition and temporal dynamics of host immune activation.

A robust hepatic response was already evident at 6 hpi, with both trophozoite clones inducing substantial transcriptional changes. The number of differentially expressed genes peaked at 12 hpi and declined by 24 hpi, indicating transient but vigorous activation of liver immune signalling, which is consistent with previous reports [28,29]. Notably, this difference was most pronounced at 12 hpi, where B2^{p} infection resulted in a markedly higher number of differentially expressed genes compared to A1^{np}.

One limitation of this study is the absence of a sham-injected control group. Because the intrahepatic injection procedure itself may induce local tissue injury and early inflammatory or stress responses, transcriptional changes observed in comparisons of infected mice with untreated controls cannot be attributed exclusively to the parasite. We therefore interpret

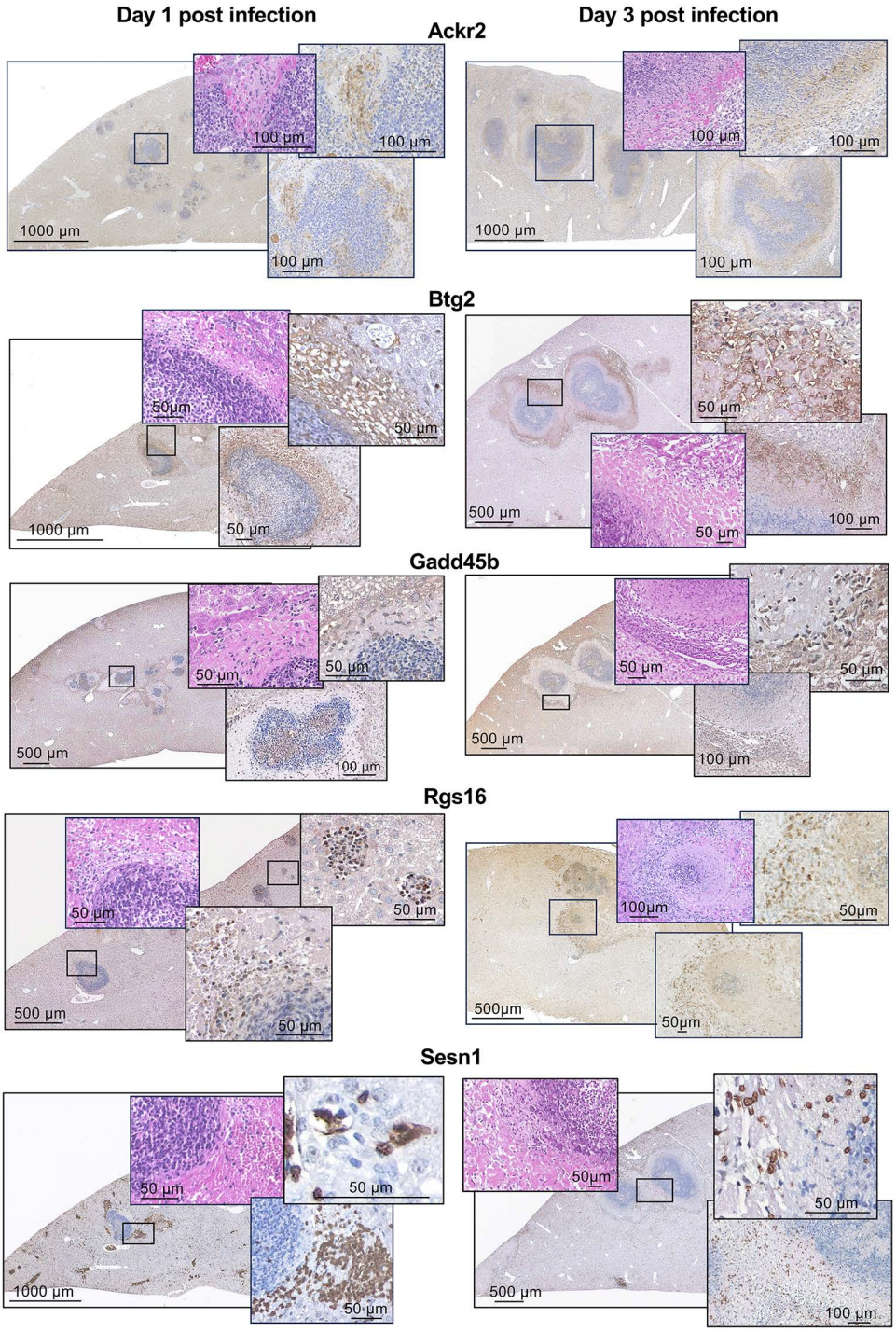


Fig 9. Localisation of Ackr2, Btg2, Gadd45b, Rgs16 and Sesn1 on immune cells one and three days after male mice were infected with B2^{P} trophozoites. Slices of paraffin-embedded liver sections from B2^{P} trophozoites-infected male mice obtained at day 1 and 3 post infection were stained with H&E or with polyclonal rabbit antibodies directed against Ackr2, Btg2, Gadd45b, Rgs16, and Sesn1. Signal detection was carried out with an anti-rabbit HRP polymer system.

https://doi.org/10.1371/journal.pntd.0014869.g009

these comparisons as infection-associated responses that may include procedure-related effects. Importantly, both A1^{np}- and B2^{p}-infected mice underwent the same intrahepatic injection procedure. For this reason, the direct A1^{np}-versus-B2^{p} comparison was used as the primary basis for conclusions regarding clone-dependent host responses, because the procedural background is shared between the two infection conditions. This comparison revealed only 12 differentially expressed genes at 6 hpi, but 543 at 12 hpi and 836 at 24 hpi, supporting a progressive clone-dependent divergence over time. Nevertheless, without a sham-injected group, procedure-specific effects common to both infected groups cannot be separated from parasite-induced responses, and this remains an important limitation of the study.

Previous studies have primarily focused on infections involving B2^{p} trophozoites, demonstrating rapid infiltration of immune cells, particularly neutrophils and monocytes, into infected liver tissue. This contributes to both parasite control and tissue injury [2,7]. Sellau *et al.* identified this cellular infiltration as a key driver of amoebic liver pathology [28]. Monocytes play a particularly important role, as an imbalance in their responses can disrupt immune homeostasis and promote pathological inflammation [2,10]. In line with these observations, our data show that B2^{p} infection is associated with the sustained induction of chemokines such as *Ccl2*, *Ccl3*, *Ccl4*, *Cxcl1*, *Cxcl2*, and *Cxcl3*. This suggests the prolonged recruitment of innate immune cells. These findings are consistent with a more persistent inflammatory environment rather than a transient response.

Extracellular vesicles (EVs) derived from *E. histolytica* may contribute to liver pathology, as they have been shown to induce pro-inflammatory immune signalling in murine monocytes, including chemokine expression and activation of TNF pathways [6]. Notably, EVs from both A1^{np} and B2^{p} trophozoites have been reported to trigger such responses, suggesting that early immune activation may be a common feature of amoebic infection. In this context, the differences observed in our study are probably due to variations in the magnitude, persistence and downstream regulation of these responses, rather than to distinct initial activation mechanisms.

Transcriptomic analysis of the liver at 6 hpi, both A1^{np} and B2^{p} *E. histolytica* trophozoites revealed an increase of a conserved set of hepatic immune and stress responses. These responses are indicative of parasite recognition via pattern recognition receptors, such as Toll-like and cytokine receptors [30,31]. This shared early response suggests activation of a common hepatic alarm programme. However, qualitative differences between the two infections were already apparent at this stage. Infection with A1^{np} trophozoites initiates a metabolically integrated immune programme characterized by the moderate activation of inflammatory and stress pathways within a regulatory context. This results in a stabilized cellular response that emphasizes metabolism, cytoprotection, and moderate immune activation. In contrast, B2^{p} trophozoites provoke a more differentiated and systemic immune response. This includes the activation of TLR receptor cascades alongside p53 and insulin signalling, increased interleukin activity, and early inflammatory amplification [32,33]. This profile indicates an early shift toward enhanced inflammatory activation and cellular stress, consistent with the development of tissue pathology [28].

By 12 hpi, infection with the non-pathogenic A1^{np} clone was associated with the coordinated enrichment of pathways related to cytokine signalling, complement activation, and coagulation, as well as chemokine-mediated immune cell recruitment, as identified by KEGG and Reactome pathway analysis. These pathways are commonly linked to early innate immune responses and inflammatory regulation [34–36]. In addition, enrichment of IL-17 signalling pathways suggests the involvement of neutrophil-driven responses and acute inflammation, particularly at epithelial interfaces [37,38]. Together with the observed modulation of lipid and steroid metabolism, these findings indicate a coordinated host response that integrates immune activation with metabolic adaptation, a pattern generally associated with the maintenance of tissue integrity during controlled inflammation [39,40]. In contrast, infection with B2^{p} trophozoites, was characterised by a stronger activation of cell-intrinsic signalling pathways, including Toll-like receptor (TLR) pathways, notably TLR3 and TLR4, as well as robust cytokine signalling and activation of central downstream cascades, including NF-κB and MAPK [30,41]. Enrichment of AGE-RAGE and TNF signalling pathways indicates oxidative stress, inflammation-driven apoptosis, and DNA damage [42,43]. Furthermore, activation of mechanosensitive pathways, such

as “fluid shear stress and atherosclerosis” suggests disturbances in vascular integrity and sinusoidal microarchitecture [44,45]. These transcriptional changes are consistent with extensive metabolic reprogramming, cell cycle arrest, and the onset of insulin resistance, all of which are associated with tissue injury and disease progression [46]. The divergence between A1^{np} and B2^{p} infection appears to arise not from the presence or absence of these specific pathways, but rather from differences in their regulation, intensity, and integration within the overall host response. While A1^{np} drives a balanced and coordinated immune response, B2^{p} triggers a more pronounced and potentially dysregulated cellular stress response.

At 24 hpi, A1^{np} infection elicts to a balanced, non-pathogenic immune response associated with activation of metabolic and cytoprotective pathways, including those involved in lipid, steroid and vitamin A metabolism, as well as platelet-associated immunomodulatory processes [40,47]. Overall, the response is controlled and non-escalatory, exhibiting regenerative features.

In comparison, B2^{p} infection at 24 hpi showed sustained activation of pro-inflammatory pathways, including cytokine and chemokine signalling, NF-κB, TNF, and complement cascades [48–51]. This persistent inflammatory state was accompanied by continued immune cell recruitment and a lack of compensatory detoxification responses, indicating ongoing tissue stress and damage [31,52–54]. These findings are consistent with previous observations that liver regeneration occurs more rapidly following A1^{np} infection than after B2^{p} infection [18].

Sex-specific factors may further modulate these responses. Since hepatic amoebiasis predominantly affects males [55], all experiments in this study were performed using male mice [4]. HIF-1α has been identified as a key regulator of sex-dependent immune responses. It promotes Th17 polarisation while limiting Treg-mediated control, thereby enhancing inflammation-induced tissue damage [56]. In addition, testosterone has been shown to enhance the recruitment of neutrophils and monocytes via CXCL1, as well as modulating interferon responses and further amplifying inflammatory processes [7,9,28]. These mechanisms may contribute to the pronounced hyperinflammatory phenotype observed in B2^{p} infection. Because only male mice were included in the present study, the extent to which the observed clone-dependent transcriptional responses can be generalized to females remains unclear. Given the known sex-dependent differences in hepatic amoebiasis and immune regulation, future studies including both sexes will be required to determine whether the identified response patterns are conserved or sex-specific.

To further dissect the molecular basis of these responses, we analysed the expression of immune-related genes. Although both A1^{np} and B2^{p} infection activated cytokine and chemokine signalling pathways, expression levels were generally higher following B2^{p} infection. Among the 151 immune-related genes, the majority displayed increased expression in B2^{p}-infected livers, indicating stronger and more complex immune activation.

At 6 hpi, both groups exhibited upregulation of genes involved in pathogen recognition and inflammatory signalling, including *Clec4e* and *Cd14* as well as chemokines such as *Cxcl2*, the immunemetabolic regulator *Acod1* and the protease inhibitors *Serpina3n*/*m* [57–62].

Concurrent induction of regulatory genes such as *Cd300lf*, *Irak3*, and *Cd33* indicates early activation of feedback mechanisms limiting excessive inflammation [63–65].

However, distinct differences were already evident. A1^{np} infection showed stronger induction of acute-phase and antimicrobial genes, including *Serpine1*, *Lcn2*, and *Cxcl2*, suggesting rapid activation of innate defence mechanisms [66–69]. In contrast, B2^{p} infection resulted in heightened expression of genes promoting inflammation (*Osm*, *Rgs16*, *Igfbp1*), cellular stress responses (*Gadd45b*, *Gadd45g*, *Txnip*) and leukocyte recruitment (*Cxcl3*, *Mmp8*) [70–76].

At 12 hpi, both groups sustained activation of innate immune pathways, particularly those associated with neutrophil recruitment, as indicated by expression of *Cxcl1* and *Cxcr4* [77,78]. Simultaneously, regulatory genes such as *Il1rn* and Serpina3m were upregulated, suggesting ongoing control of inflammatory damage [79,80].

B2^{p} infection, however, was characterized by stronger induction of inflammatory and stress-related genes, including *Il17ra*, *Cxcl2*, *Ccr1*, and *Cxcr2*, and members of the *Gadd45* family [69,75,81–86]. This was accompanied by increased

expression of *Il1r1*, *Tnfrsf1b*, *Phf11c*, and *Rgs16*, collectively indicating enhanced cytokine receptor signalling and immune cell activation [71,87–90]. At the same time, regulatory genes associated with immune-dampening mechanisms, such as *Il1r2*, *Setdb2*, and *Ackr2*, were also upregulated, suggesting the concurrent activation of compensatory feedback pathways aimed at restraining excessive inflammation [91–94].

By 24 hpi, both groups exhibited signs of immune resolution, stabilised by anti-inflammatory signalling and tissue repair. This included the induction of anti-inflammatory and regulatory genes, such as *Hp*, *Cish*, *Cd33* and *Gas6*, as well as the coordinated regulation of genes involved in immune cell trafficking, maturation and adhesion (*Cxcr4*, *Itgam*, *Csf3r*) [78,95–101].

However, B2^{p} infection was characterised by markedly elevated expression of pro-inflammatory and acute-phase mediators, including *Cxcl2*, *Cxcl3*, *Ccl3*, *Saa3*, *Osm*, *Ptgs2* and *Trem1*. This indicates sustained immune activation and ongoing tissue stress [67,69,70,73,102,103]. The persistently high expression of *Il1r2* suggested sustained anti-inflammatory feedback. Meanwhile, the elevated levels of *Serpine1* possibly contributed to tissue protection and the resolution of inflammation [91,92].

In our study, immunohistochemical staining revealed distinct spatial patterns of cells expressing genes that were strongly up-regulated during B2^{p} infection. Cells positive for Ackr2, Btg2 and Sesn1 accumulated predominantly at the periphery of the amoebic abscess, whereas cells expressing Gadd45b and Rgs16 were located more centrally, in closer proximity to the trophozoites. These spatial differences may reflect distinct functional programmes within the inflammatory lesion.

Ackr2 (atypical chemokine receptor 2) acts as a chemokine-scavenging receptor that sequesters and degrades excessive chemokine levels [28,29], thereby helping to limit dysregulated chemokine-driven inflammation. *Rgs16* (regulator of G-protein signalling 16) modulates G-protein-coupled receptor signalling and may thereby influence inflammatory signalling and immune-cell positioning [30]. In addition to these regulators of inflammatory signalling, *Btg2* (B-cell translocation gene 2) contributes to the control of cell-cycle progression and stress responses [31], *Gadd45b* (Growth Arrest and DNA Damage-inducible 45 beta) is involved in cellular responses to environmental and genotoxic stress as well as DNA-damage regulation [32], and *Sesn1* (Sestrin 1) functions as a sensor of cellular stress, particularly oxidative stress, and contributes to redox homeostasis [33]. The distinct spatial distribution of cells expressing these proteins within the amoebic liver abscess may reflect these different functional roles. Cells positive for Ackr2, Btg2 and Sesn1 accumulated predominantly at the abscess margin, a localisation consistent with regulatory and stress-protective functions that may help to limit excessive inflammatory damage and stabilise the surrounding tissue. In contrast, Gadd45b- and Rgs16-positive cells were enriched closer to the parasite–host interface. Given the roles of Gadd45b in stress-associated signalling and of Rgs16 in GPCR-mediated responses, their central localisation may reflect stronger engagement of stress-response and effector programmes in regions directly exposed to trophozoites [77,89]. Together, these findings suggest a spatial organisation of immune regulatory and stress-response programmes within the amoebic liver abscess, with more regulatory and protective responses at the lesion periphery and stress-associated responses closer to the parasite-rich centre.

The clone-dependent regulation of factors such as Ackr2, Gadd45b and Rgs16 may also have translational relevance. Ackr2 is involved in the control of chemokine availability and may therefore represent a potential node for modulating excessive inflammatory cell recruitment. Gadd45b and Rgs16, which were associated with stress-response and signalling programmes in B2^{p}-infected livers, may likewise reflect pathways involved in the transition from controlled inflammation to tissue-damaging responses. These molecules could therefore be considered as candidates for future studies investigating host-directed therapeutic strategies aimed at limiting immunopathology without impairing parasite control. In addition, their distinct temporal and spatial regulation raises the possibility that they may serve as markers of inflammatory state or disease progression. However, their value as therapeutic targets or biomarkers remains speculative and will require validation in independent experimental studies.

Conclusion

This study reveals that the immune response to *E. histolytica* in the liver is shaped by both conserved core pathways and clone-specific dynamics. While both clones activate innate defences, including cytokines, chemokines and regulatory feedback, the non-pathogenic A1^{np} clone triggers a rapid but self-limiting inflammatory response involving antimicrobial defence and tissue protection. By contrast, the pathogenic B2^{p} clone provokes a more sustained and multifaceted pro-inflammatory immune response characterised by oxidative stress, cytokine amplification and tissue remodelling. These findings suggest that immune dysregulation in response to distinct parasitic clones, rather than parasite presence alone, is a key driver of liver pathology in ALA. Understanding these divergent immune profiles could inform future therapies aimed at mitigating tissue damage by modulating host responses without compromising pathogen control.

Supporting information

S1 Table. Overview of transcriptomic datasets: expression browser and differential gene expression analyses across infection conditions and time points. Sheet 1: Expression Browser; Sheet 2–4: A1^{np} vs Control (6, 12, 24 hpi); Sheet 5–7: B2^{p} vs Control (6, 12, 24 hpi); Sheet 8–10: B2^{p} vs A1^{np} (6, 12, 24 hpi).
(XLSX)

S2 Table. Overview of transcriptomic datasets for 151 immune system–associated genes (Sheet 1) and the expression browser (Sheet 2).
(XLSX)

S3 Table. Differential gene expression of 151 immune-related genes in liver tissue following infection with A1^{np} and B2^{p} trophozoites.
(DOCX)

Acknowledgments

We would like to thank Susann Ofori for her technical assistance and excellent laboratory management.

Author contributions

Conceptualization: Helena Fehling, Hannelore Lotter, Iris Bruchhaus.

Data curation: Helena Fehling, Johannes Allweier, Iris Bruchhaus.

Formal analysis: Helena Fehling, Johannes Allweier, Barbara Honecker, Iris Bruchhaus.

Funding acquisition: Hannelore Lotter, Iris Bruchhaus.

Investigation: Helena Fehling, Johannes Allweier, Claudia Marggraff.

Methodology: Helena Fehling, Claudia Marggraff.

Supervision: Hannelore Lotter, Iris Bruchhaus.

Visualization: Johannes Allweier, Barbara Honecker, Iris Bruchhaus.

Writing – original draft: Iris Bruchhaus.

Writing – review & editing: Helena Fehling, Johannes Allweier, Barbara Honecker, Michel-Ruben Glagowski, Juliett Anders, Hannelore Lotter, Iris Bruchhaus.

References

1. GBD 2016 Diarrhoeal Disease Collaborators. Estimates of the global, regional, and national morbidity, mortality, and aetiologies of diarrhoea in 195 countries: a systematic analysis for the Global Burden of Disease Study 2016. Lancet Infect Dis. 2018;18(11):1211–28. https://doi.org/10.1016/S1473-3099(18)30362-1 PMID: 30243583
2. Helk E, Bernin H, Ernst T, Ittrich H, Jacobs T, Heeren J, et al. TNFα-mediated liver destruction by Kupffer cells and Ly6Chi monocytes during Entamoeba histolytica infection. PLoS Pathog. 2013;9(1):e1003096. https://doi.org/10.1371/journal.ppat.1003096 PMID: 23300453
3. Estrada-Figueroa LA, Ramírez-Jiménez Y, Osorio-Trujillo C, Shibayama M, Navarro-García F, García-Tovar C, et al. Absence of CD38 delays arrival of neutrophils to the liver and innate immune response development during hepatic amoebiasis by Entamoeba histolytica. Parasite Immunol. 2011;33(12):661–8. https://doi.org/10.1111/j.1365-3024.2011.01333.x PMID: 21919917
4. Lotter H, Jacobs T, Gaworski I, Tannich E. Sexual dimorphism in the control of amebic liver abscess in a mouse model of disease. Infection and Immunity. 2006;74(1):118–24. PMID: 16368964
5. Pacheco-Yépez J, Galván-Moroyoqui JM, Meza I, Tsutsumi V, Shibayama M. Expression of cytokines and their regulation during amoebic liver abscess development. Parasite Immunol. 2011;33(1):56–64. https://doi.org/10.1111/j.1365-3024.2010.01252.x PMID: 21155843
6. Honecker B, Bärreiter VA, Höhn K, Horváth B, Harant K, Metwally NG, et al. Entamoeba histolytica extracellular vesicles drive pro-inflammatory monocyte signaling. PLoS Negl Trop Dis. 2025;19(4):e0012997. https://doi.org/10.1371/journal.pntd.0012997 PMID: 40208874
7. Er-Lukowiak M, Hänzelmann S, Rothe M, Moamenpour DT, Hausmann F, Khatri R, et al. Testosterone affects type I/type II interferon response of neutrophils during hepatic amebiasis. Front Immunol. 2023;14:1279245. https://doi.org/10.3389/fimmu.2023.1279245 PMID: 38179044
8. García-Zepeda EA, Rojas-López A, Esquivel-Velázquez M, Ostoa-Saloma P. Regulation of the inflammatory immune response by the cytokine/chemokine network in amoebiasis. Parasite Immunol. 2007;29(12):679–84. https://doi.org/10.1111/j.1365-3024.2007.00990.x PMID: 18042174
9. Sellau J, Groneberg M, Fehling H, Thye T, Hoenow S, Marggraff C, et al. Androgens predispose males to monocyte-mediated immunopathology by inducing the expression of leukocyte recruitment factor CXCL1. Nat Commun. 2020;11(1):3459. https://doi.org/10.1038/s41467-020-17260-y PMID: 32651360
10. Sellau J, Puengel T, Hoenow S, Groneberg M, Tacke F, Lotter H. Monocyte dysregulation: consequences for hepatic infections. Semin Immunopathol. 2021;43(4):493–506. https://doi.org/10.1007/s00281-021-00852-1 PMID: 33829283
11. Maldonado-Bernal C, Kirschning CJ, Rosenstein Y, Rocha LM, Rios-Sarabia N, Espinosa-Cantellano M, et al. The innate immune response to Entamoeba histolytica lipopeptidophosphoglycan is mediated by toll-like receptors 2 and 4. Parasite Immunol. 2005;27(4):127–37. https://doi.org/10.1111/j.1365-3024.2005.00754.x PMID: 15910421
12. Faust DM, Marquay Markiewicz J, Santi-Rocca J, Guillen N. New insights into host-pathogen interactions during Entamoeba histolytica liver infection. Eur J Microbiol Immunol (Bp). 2011;1(1):10–8. https://doi.org/10.1556/EuJMI.1.2011.1.4 PMID: 24466432
13. Begum S, Quach J, Chadee K. Immune evasion mechanisms of Entamoeba histolytica: progression to disease. Front Microbiol. 2015;6:1394. https://doi.org/10.3389/fmicb.2015.01394 PMID: 26696997
14. Fonseca Z, Díaz-Godínez C, Mora N, Alemán OR, Uribe-Querol E, Carrero JC, et al. Entamoeba histolytica induce signaling via Raf/MEK/ERK for Neutrophil Extracellular Trap (NET) Formation. Front Cell Infect Microbiol. 2018;8:226. https://doi.org/10.3389/fcimb.2018.00226 PMID: 30023352
15. Ávila EE, Salaiza N, Pulido J, Rodríguez MC, Díaz-Godínez C, Laclette JP, et al. Entamoeba histolytica Trophozoites and Lipopeptidophosphoglycan trigger human neutrophil extracellular traps. PLoS One. 2016;11(7):e0158979. https://doi.org/10.1371/journal.pone.0158979 PMID: 27415627
16. Roy M, Chakraborty S, Kumar Srivastava S, Kaushik S, Jyoti A, Kumar Srivastava V. Entamoeba histolytica induced NETosis and the dual role of NETs in amoebiasis. Int Immunopharmacol. 2023;118:110100. https://doi.org/10.1016/j.intimp.2023.110100 PMID: 37011501
17. Díaz-Godínez C, Ríos-Valencia DG, García-Aguirre S, Martínez-Calvillo S, Carrero JC. Immunomodulatory effect of extracellular vesicles from Entamoeba histolytica trophozoites: Regulation of NETs and respiratory burst during confrontation with human neutrophils. Front Cell Infect Microbiol. 2022;12:1018314. https://doi.org/10.3389/fcimb.2022.1018314 PMID: 36389143
18. Meyer M, Fehling H, Matthiesen J, Lorenzen S, Schuldt K, Bernin H, et al. Overexpression of differentially expressed genes identified in non-pathogenic and pathogenic Entamoeba histolytica clones allow identification of new pathogenicity factors involved in amoebic liver abscess formation. PLoS Pathog. 2016;12(8):e1005853. https://doi.org/10.1371/journal.ppat.1005853 PMID: 27575775
19. König C, Honecker B, Wilson IW, Weedall GD, Hall N, Roeder T, et al. Taxon-specific proteins of the pathogenic entamoeba species *E. histolytica* and *E. nuttalli*. Front Cell Infect Microbiol. 2021;11:641472. https://doi.org/10.3389/fcimb.2021.641472 PMID: 33816346
20. Petri WA, Schnaar RL. Purification and characterization of galactose- and N-acetylgalactosamine-specific adhesin lectin of Entamoeba histolytica. Methods Enzymol. 1995;253:98–104.
21. Matthiesen J, Bär A-K, Bartels A-K, Marien D, Ofori S, Biller L, et al. Overexpression of specific cysteine peptidases confers pathogenicity to a nonpathogenic Entamoeba histolytica clone. mBio. 2013;4(2):e00072-13. https://doi.org/10.1128/mBio.00072-13 PMID: 23532975
22. Leippe M. Amoebapores. Parasitol Today. 1997;13(5):178–83.
23. Matthiesen J, Lender C, Haferkorn A, Fehling H, Meyer M, Matthies T, et al. Trigger-induced RNAi gene silencing to identify pathogenicity factors of Entamoeba histolytica. FASEB J. 2019;33(2):1658–68. https://doi.org/10.1096/fj.201801313R PMID: 30169111
24. Diamond LS, Harlow DR, Cunnick CC. A new medium for the axenic cultivation of Entamoeba histolytica and other Entamoeba. Trans R Soc Trop Med Hyg. 1978;72(4):431–2. https://doi.org/10.1016/0035-9203(78)90144-x PMID: 212851

25. Babicki S, Arndt D, Marcu A, Liang Y, Grant JR, Maciejewski A, et al. Heatmapper: web-enabled heat mapping for all. Nucleic Acids Res. 2016;44(W1):W147-53. https://doi.org/10.1093/nar/gkw419 PMID: 27190236
26. Szklarczyk D, Kirsch R, Koutrouli M, Nastou K, Mehryary F, Hachilif R, et al. The STRING database in 2023: protein-protein association networks and functional enrichment analyses for any sequenced genome of interest. Nucleic Acids Res. 2023;51(D1):D638–46. https://doi.org/10.1093/nar/gkac1000 PMID: 36370105
27. Galaxy Community. The Galaxy platform for accessible, reproducible, and collaborative data analyses: 2024 update. Nucleic Acids Res. 2024;52(W1):W83–94. https://doi.org/10.1093/nar/gkae410 PMID: 38769056
28. Sellau J, Groneberg M, Hoenow S, Lotter H. The underlying cellular immune pathology of Entamoeba histolytica-induced hepatic amoebiasis. J Hepatol. 2021;75(2):481–2. https://doi.org/10.1016/j.jhep.2021.03.018 PMID: 34120776
29. Pulido-Ortega J, Talamas-Rohana P, Munoz-Ortega MH, Aldaba-Muruato LR, Martinez-Hernandez SL, Campos-Esparza MDR, et al. Functional characterization of an interferon gamma receptor-like protein on Entamoeba histolytica. Infection and immunity. 2019;87(11). https://doi.org/10.1128/IAI.00540-19 PMID: 31427448
30. Duan T, Du Y, Xing C, Wang HY, Wang R-F. Toll-like receptor signaling and its role in cell-mediated immunity. Front Immunol. 2022;13:812774. https://doi.org/10.3389/fimmu.2022.812774 PMID: 35309296
31. Kiziltas S. Toll-like receptors in pathophysiology of liver diseases. World J Hepatol. 2016;8(32):1354–69. https://doi.org/10.4254/wjh.v8.i32.1354 PMID: 27917262
32. Chen L, Deng H, Cui H, Fang J, Zuo Z, Deng J, et al. Inflammatory responses and inflammation-associated diseases in organs. Oncotarget. 2017;9(6):7204–18. https://doi.org/10.18632/oncotarget.23208 PMID: 29467962
33. Salauddin M, Bhattacharyya D, Samanta I, Saha S, Xue M, Hossain MG, et al. Role of TLRs as signaling cascades to combat infectious diseases: a review. Cell Mol Life Sci. 2025;82(1):122. https://doi.org/10.1007/s00018-025-05631-x PMID: 40105962
34. Huber-Lang M, Kovtun A, Ignatius A. The role of complement in trauma and fracture healing. Semin Immunol. 2013;25(1):73–8. https://doi.org/10.1016/j.smim.2013.05.006 PMID: 23768898
35. Czermak BJ, Lentsch AB, Bless NM, Schmal H, Friedl HP, Ward PA. Synergistic enhancement of chemokine generation and lung injury by C5a or the membrane attack complex of complement. Am J Pathol. 1999;154(5):1513–24. https://doi.org/10.1016/S0002-9440(10)65405-3 PMID: 10329604
36. Diaz-Valencia JD, Pérez-Yépez EA, Ayala-Sumuano JT, Franco E, Meza I. A surface membrane protein of Entamoeba histolytica functions as a receptor for human chemokine IL-8: its role in the attraction of trophozoites to inflammation sites. Int J Parasitol. 2015;45(14):915–23. https://doi.org/10.1016/j.ijpara.2015.07.007 PMID: 26343219
37. Paquissi FC. Immune imbalances in non-alcoholic fatty liver disease: from general biomarkers and neutrophils to interleukin-17 axis activation and new therapeutic targets. Front Immunol. 2016;7:490. https://doi.org/10.3389/fimmu.2016.00490 PMID: 27891128
38. Shen H, Liangpunsakul S, Iwakiri Y, Szabo G, Wang H. Immunological mechanisms and emerging therapeutic targets in alcohol-associated liver disease. Cell Mol Immunol. 2025;22(10):1190–204. https://doi.org/10.1038/s41423-025-01291-w PMID: 40399593
39. Rudnick DA, Davidson NO. Functional relationships between lipid metabolism and liver regeneration. Int J Hepatol. 2012;2012:549241. https://doi.org/10.1155/2012/549241 PMID: 22319652
40. Garcia C, Andersen CJ, Blesso CN. The role of lipids in the regulation of immune responses. Nutrients. 2023;15(18):3899. https://doi.org/10.3390/nu15183899 PMID: 37764683
41. Kawai T, Ikegawa M, Ori D, Akira S. Decoding Toll-like receptors: Recent insights and perspectives in innate immunity. Immunity. 2024;57(4):649–73. https://doi.org/10.1016/j.immuni.2024.03.004 PMID: 38599164
42. Zhou M, Zhang Y, Shi L, Li L, Zhang D, Gong Z, et al. Activation and modulation of the AGEs-RAGE axis: Implications for inflammatory pathologies and therapeutic interventions - A review. Pharmacol Res. 2024;206:107282. https://doi.org/10.1016/j.phrs.2024.107282 PMID: 38914383
43. Yue Q, Song Y, Liu Z, Zhang L, Yang L, Li J. Receptor for Advanced Glycation End Products (RAGE): a pivotal hub in immune diseases. Molecules. 2022;27(15):4922. https://doi.org/10.3390/molecules27154922 PMID: 35956875
44. Cheng H, Zhong W, Wang L, Zhang Q, Ma X, Wang Y, et al. Effects of shear stress on vascular endothelial functions in atherosclerosis and potential therapeutic approaches. Biomed Pharmacother. 2023;158:114198. https://doi.org/10.1016/j.biopha.2022.114198 PMID: 36916427
45. Conway DE, Schwartz MA. Flow-dependent cellular mechanotransduction in atherosclerosis. J Cell Sci. 2013;126(Pt 22):5101–9. https://doi.org/10.1242/jcs.138313 PMID: 24190880
46. Malhi H, Gores GJ. Cellular and molecular mechanisms of liver injury. Gastroenterology. 2008;134(6):1641–54. https://doi.org/10.1053/j.gastro.2008.03.002 PMID: 18471544
47. Lisman T, Luyendyk JP. Platelets as modulators of liver diseases. Semin Thromb Hemost. 2018;44(2):114–25. https://doi.org/10.1055/s-0037-1604091 PMID: 28898899
48. Tak PP, Firestein GS. NF-kappaB: a key role in inflammatory diseases. J Clin Invest. 2001;107(1):7–11. https://doi.org/10.1172/JCI11830 PMID: 11134171
49. Bhol NK, Bhanjadeo MM, Singh AK, Dash UC, Ojha RR, Majhi S, et al. The interplay between cytokines, inflammation, and antioxidants: mechanistic insights and therapeutic potentials of various antioxidants and anti-cytokine compounds. Biomed Pharmacother. 2024;178:117177. https://doi.org/10.1016/j.biopha.2024.117177 PMID: 39053423

50. Dorrington MG, Fraser IDC. NF-κB signaling in macrophages: dynamics, crosstalk, and signal integration. Front Immunol. 2019;10:705. https://doi.org/10.3389/fimmu.2019.00705 PMID: 31024544
51. Tacke F, Luedde T, Trautwein C. Inflammatory pathways in liver homeostasis and liver injury. Clin Rev Allergy Immunol. 2009;36(1):4–12. https://doi.org/10.1007/s12016-008-8091-0 PMID: 18600481
52. Robinson MW, Harmon C, O'Farrelly C. Liver immunology and its role in inflammation and homeostasis. Cell Mol Immunol. 2016;13(3):267–76. https://doi.org/10.1038/cmi.2016.3 PMID: 27063467
53. Martin-Mateos R, Alvarez-Mon M, Albillos A. Dysfunctional immune response in acute-on-chronic liver failure: it takes two to tango. Front Immunol. 2019;10:973. https://doi.org/10.3389/fimmu.2019.00973 PMID: 31118937
54. Nakamoto N, Kanai T. Role of toll-like receptors in immune activation and tolerance in the liver. Front Immunol. 2014;5:221. https://doi.org/10.3389/fimmu.2014.00221 PMID: 24904576
55. Blessmann J, Van Linh P, Nu PAT, Thi HD, Muller-Myhsok B, Buss H, et al. Epidemiology of amebiasis in a region of high incidence of amebic liver abscess in central Vietnam. Am J Trop Med Hyg. 2002;66(5):578–83. https://doi.org/10.4269/ajtmh.2002.66.578 PMID: 12201594
56. Groneberg M, Hoenow S, Marggraff C, Fehling H, Metwally NG, Hansen C, et al. HIF-1α modulates sex-specific Th17/Treg responses during hepatic amoebiasis. J Hepatol. 2022;76(1):160–73. https://doi.org/10.1016/j.jhep.2021.09.020 PMID: 34599999
57. Pahari S, Negi S, Aqdas M, Arnett E, Schlesinger LS, Agrewala JN. Induction of autophagy through CLEC4E in combination with TLR4: an innovative strategy to restrict the survival of Mycobacterium tuberculosis. Autophagy. 2020;16(6):1021–43. https://doi.org/10.1080/15548627.2019.1658436 PMID: 31462144
58. Na K, Oh B-C, Jung Y. Multifaceted role of CD14 in innate immunity and tissue homeostasis. Cytokine Growth Factor Rev. 2023;74:100–7. https://doi.org/10.1016/j.cytogfr.2023.08.008 PMID: 37661484
59. Ding L, Hayes MM, Photenhauer A, Eaton KA, Li Q, Ocadiz-Ruiz R, et al. Schlafen 4-expressing myeloid-derived suppressor cells are induced during murine gastric metaplasia. J Clin Invest. 2016;126(8):2867–80. https://doi.org/10.1172/JCI82529 PMID: 27427984
60. De Filippo K, Henderson RB, Laschinger M, Hogg N. Neutrophil chemokines KC and macrophage-inflammatory protein-2 are newly synthesized by tissue macrophages using distinct TLR signaling pathways. J Immunol. 2008;180(6):4308–15. https://doi.org/10.4049/jimmunol.180.6.4308 PMID: 18322244
61. Wu R, Liu J, Tang D, Kang R. The dual role of ACOD1 in inflammation. J Immunol. 2023;211(4):518–26. https://doi.org/10.4049/jimmunol.2300101 PMID: 37549395
62. de Mezer M, Rogaliński J, Przewoźny S, Chojnicki M, Niepolski L, Sobieska M, et al. SERPINA3: stimulator or inhibitor of pathological changes. Biomedicines. 2023;11(1):156. https://doi.org/10.3390/biomedicines11010156 PMID: 36672665
63. Sutherland SIM, Ju X, Silveira PA, Kupresanin F, Horvath LG, Clark GJ. CD300f signalling induces inhibitory human monocytes/macrophages. Cell Immunol. 2023;390:104731. https://doi.org/10.1016/j.cellimm.2023.104731 PMID: 37302321
64. Freihat LA, Wheeler JI, Wong A, Turek I, Manallack DT, Irving HR. IRAK3 modulates downstream innate immune signalling through its guanylate cyclase activity. Sci Rep. 2019;9(1):15468. https://doi.org/10.1038/s41598-019-51913-3 PMID: 31664109
65. Lajaunias F, Dayer J-M, Chizzolini C. Constitutive repressor activity of CD33 on human monocytes requires sialic acid recognition and phosphoinositide 3-kinase-mediated intracellular signaling. Eur J Immunol. 2005;35(1):243–51. https://doi.org/10.1002/eji.200425273 PMID: 15597323
66. Kubota M, Yoshida Y, Kobayashi E, Matsutani T, Li S-Y, Zhang B-S, et al. Serum anti-SERPINE1 antibody as a potential biomarker of acute cerebral infarction. Sci Rep. 2021;11(1):21772. https://doi.org/10.1038/s41598-021-01176-8 PMID: 34741085
67. Brusletto BS, Løberg EM, Hellerud BC, Goverud IL, Berg JP, Olstad OK, et al. Extensive changes in transcriptomic "fingerprints" and immunological cells in the large organs of patients dying of acute septic shock and multiple organ failure caused by neisseria meningitidis. Front Cell Infect Microbiol. 2020;10:42. https://doi.org/10.3389/fcimb.2020.00042 PMID: 32154187
68. Chang Y-L, Wang Z, Igawa S, Choi JE, Werbel T, Di Nardo A. Lipocalin 2: a new antimicrobial in mast cells. Int J Mol Sci. 2019;20(10):2380. https://doi.org/10.3390/ijms20102380 PMID: 31091692
69. Lv Y, Chen C, Han M, Tian C, Song F, Feng S, et al. CXCL2: a key player in the tumor microenvironment and inflammatory diseases. Cancer Cell Int. 2025;25(1):133. https://doi.org/10.1186/s12935-025-03765-3 PMID: 40197328
70. Wolf CL, Pruett C, Lighter D, Jorcyk CL. The clinical relevance of OSM in inflammatory diseases: a comprehensive review. Front Immunol. 2023;14:1239732. https://doi.org/10.3389/fimmu.2023.1239732 PMID: 37841259
71. Zhu F, Qin Y, Wang Y, Zhang F, Xu Z, Dai F, et al. Critical roles of RGS16 in the mucosal inflammation of ulcerative colitis. Eur J Gastroenterol Hepatol. 2022;34(10):993–9. https://doi.org/10.1097/MEG.0000000000002407 PMID: 35830366
72. Lewitt MS, Boyd GW. Insulin-like Growth Factor-Binding Protein-1 (IGFBP-1) as a biomarker of cardiovascular disease. Biomolecules. 2024;14(11):1475. https://doi.org/10.3390/biom14111475 PMID: 39595651
73. Bao Y, Tong C, Xiong X. CXCL3: A key player in tumor microenvironment and inflammatory diseases. Life Sci. 2024;348:122691. https://doi.org/10.1016/j.lfs.2024.122691 PMID: 38714265
74. Khatwa UA, Kleibrink BE, Shapiro SD, Subramaniam M. MMP-8 promotes polymorphonuclear cell migration through collagen barriers in obliterative bronchiolitis. J Leukoc Biol. 2010;87(1):69–77. https://doi.org/10.1189/jlb.0509361 PMID: 19801498
75. Liebermann DA, Hoffman B. Gadd45 in stress signaling. J Mol Signal. 2008;3:15. https://doi.org/10.1186/1750-2187-3-15 PMID: 18789159

76. Choi E-H, Park S-J. TXNIP: A key protein in the cellular stress response pathway and a potential therapeutic target. Exp Mol Med. 2023;55(7):1348–56. https://doi.org/10.1038/s12276-023-01019-8 PMID: 37394581

77. Sawant KV, Poluri KM, Dutta AK, Sepuru KM, Troshkina A, Garofalo RP, et al. Chemokine CXCL1 mediated neutrophil recruitment: Role of glycosaminoglycan interactions. Sci Rep. 2016;6:33123. https://doi.org/10.1038/srep33123 PMID: 27625115

78. De Filippo K, Rankin SM. CXCR4, the master regulator of neutrophil trafficking in homeostasis and disease. Eur J Clin Invest. 2018;48 Suppl 2(Suppl Suppl 2):e12949. https://doi.org/10.1111/eci.12949 PMID: 29734477

79. Zhang M, Huang Y, Pan J, Sang C, Lin Y, Dong L, et al. An inflammatory checkpoint generated by IL1RN splicing offers therapeutic opportunity for KRAS-mutant intrahepatic cholangiocarcinoma. Cancer Discov. 2023;13(10):2248–69. https://doi.org/10.1158/2159-8290.CD-23-0282 PMID: 37486241

80. Heit C, Jackson BC, McAndrews M, Wright MW, Thompson DC, Silverman GA, et al. Update of the human and mouse SERPIN gene superfamily. Hum Genomics. 2013;7(1):22. https://doi.org/10.1186/1479-7364-7-22 PMID: 24172014

81. Ge S, Hertel B, Susnik N, Rong S, Dittrich AM, Schmitt R, et al. Interleukin 17 receptor A modulates monocyte subsets and macrophage generation in vivo. PLoS One. 2014;9(1):e85461. https://doi.org/10.1371/journal.pone.0085461 PMID: 24454873

82. Zimmermann HW, Tacke F. Modification of chemokine pathways and immune cell infiltration as a novel therapeutic approach in liver inflammation and fibrosis. Inflamm Allergy Drug Targets. 2011;10(6):509–36. https://doi.org/10.2174/187152811798104890 PMID: 22150762

83. Salerno DM, Tront JS, Hoffman B, Liebermann DA. Gadd45a and Gadd45b modulate innate immune functions of granulocytes and macrophages by differential regulation of p38 and JNK signaling. J Cell Physiol. 2012;227(11):3613–20. https://doi.org/10.1002/jcp.24067 PMID: 22307729

84. Takekawa M, Saito H. A family of stress-inducible GADD45-like proteins mediate activation of the stress-responsive MTK1/MEKK4 MAPKKK. Cell. 1998;95(4):521–30. https://doi.org/10.1016/s0092-8674(00)81619-0 PMID: 9827804

85. Dostie KE, Thees AV, Lynes MA. Metallothionein: a novel therapeutic target for treatment of inflammatory bowel disease. Curr Pharm Des. 2018;24(27):3155–61. https://doi.org/10.2174/1381612824666180717110236 PMID: 30014800

86. Devisscher L, Hindryckx P, Lynes MA, Waeytens A, Cuvelier C, De Vos F, et al. Role of metallothioneins as danger signals in the pathogenesis of colitis. J Pathol. 2014;233(1):89–100. https://doi.org/10.1002/path.4330 PMID: 24452846

87. Auron PE. The interleukin 1 receptor: ligand interactions and signal transduction. Cytokine Growth Factor Rev. 1998;9(3–4):221–37. https://doi.org/10.1016/s1359-6101(98)00018-5 PMID: 9918122

88. Rahman N, Stewart G, Jones G. A role for the atopy-associated gene PHF11 in T-cell activation and viability. Immunol Cell Biol. 2010;88(8):817–24. https://doi.org/10.1038/icb.2010.57 PMID: 20421878

89. Gao Y, Shi H, Zhao H, Yao M, He Y, Jiang M, et al. Single-cell transcriptomics identify TNFRSF1B as a novel T-cell exhaustion marker for ovarian cancer. Clin Transl Med. 2023;13(9):e1416. https://doi.org/10.1002/ctm2.1416 PMID: 37712139

90. McCulloch TR, Rossi GR, Alim L, Lam PY, Wong JKM, Coleborn E, et al. Dichotomous outcomes of TNFR1 and TNFR2 signaling in NK cell-mediated immune responses during inflammation. Nat Commun. 2024;15(1):9871. https://doi.org/10.1038/s41467-024-54232-y PMID: 39543125

91. Supino D, Minute L, Mariancini A, Riva F, Magrini E, Garlanda C. Negative regulation of the IL-1 System by IL-1R2 and IL-1R8: relevance in pathophysiology and disease. Front Immunol. 2022;13:804641. https://doi.org/10.3389/fimmu.2022.804641 PMID: 35211118

92. Molgora M, Supino D, Mantovani A, Garlanda C. Tuning inflammation and immunity by the negative regulators IL-1R2 and IL-1R8. Immunol Rev. 2018;281(1):233–47. https://doi.org/10.1111/imr.12609 PMID: 29247989

93. Schliehe C, Flynn EK, Vilagos B, Richson U, Swaminanthan S, Bosnjak B, et al. The methyltransferase Setdb2 mediates virus-induced susceptibility to bacterial superinfection. Nat Immunol. 2015;16(1):67–74. https://doi.org/10.1038/ni.3046 PMID: 25419628

94. Hansell CAH, Fraser AR, Hayes AJ, Pingen M, Burt CL, Lee KM, et al. The atypical chemokine receptor Ackr2 constrains NK cell migratory activity and promotes metastasis. J Immunol. 2018;201(8):2510–9. https://doi.org/10.4049/jimmunol.1800131 PMID: 30158126

95. Galicia G, Maes W, Verbinnen B, Kasran A, Bullens D, Arredouani M, et al. Haptoglobin deficiency facilitates the development of autoimmune inflammation. Eur J Immunol. 2009;39(12):3404–12. https://doi.org/10.1002/eji.200939291 PMID: 19795414

96. Wang Y, Kinzie E, Berger FG, Lim SK, Baumann H. Haptoglobin, an inflammation-inducible plasma protein. Redox Rep. 2001;6(6):379–85. https://doi.org/10.1179/135100001101536580 PMID: 11865981

97. Naser W, Maymand S, Dlugolenski D, Basheer F, Ward AC. The Role of Cytokine-Inducible SH2 Domain-Containing Protein (CISH) in the regulation of basal and cytokine-mediated myelopoiesis. Int J Mol Sci. 2023;24(16):12757. https://doi.org/10.3390/ijms241612757 PMID: 37628937

98. Paul SP, Taylor LS, Stansbury EK, McVicar DW. Myeloid specific human CD33 is an inhibitory receptor with differential ITIM function in recruiting the phosphatases SHP-1 and SHP-2. Blood. 2000;96(2):483–90. https://doi.org/10.1182/blood.v96.2.483 PMID: 10887109

99. Nassar M, Tabib Y, Capucha T, Mizraji G, Nir T, Pevsner-Fischer M, et al. GAS6 is a key homeostatic immunological regulator of host-commensal interactions in the oral mucosa. Proc Natl Acad Sci U S A. 2017;114(3):E337–46. https://doi.org/10.1073/pnas.1614926114 PMID: 28049839

100. Lou Y, Li PH, Liu XQ, Wang TX, Liu YL, Chen CC, et al. ITGAM-mediated macrophages contribute to basement membrane damage in diabetic nephropathy and atherosclerosis. BMC Nephrol. 2024;25(1):72. https://doi.org/10.1186/s12882-024-03505-1 PMID: 38413872

101. Zhang H, Coblentz C, Watanabe-Smith K, Means S, Means J, Maxson JE, et al. Gain-of-function mutations in granulocyte colony-stimulating factor receptor (CSF3R) reveal distinct mechanisms of CSF3R activation. J Biol Chem. 2018;293(19):7387–96. https://doi.org/10.1074/jbc.RA118.002417 PMID: 29572350

102. Sipprell SE, Johnson MB, Leach W, Suptela SR, Marriott I. Staphylococcus aureus Infection Induces the Production of the Neutrophil Chemoattractants CXCL1, CXCL2, CXCL3, CXCL5, CCL3, and CCL7 by Murine Osteoblasts. Infect Immun. 2023;91(4):e0001423. https://doi.org/10.1128/iai.00014-23 PMID: 36880752

103. Li R, Xie J, Xu W, Zhang L, Lin H, Huang W. LPS-induced PTGS2 manipulates the inflammatory response through trophoblast invasion in preeclampsia via NF-κB pathway. Reprod Biol. 2022;22(4):100696. https://doi.org/10.1016/j.repbio.2022.100696 PMID: 36327673